3-23-2016

Assessment of the Role of Poly (ADP-Ribose) Polymerase in Drug-Induced Cardiomyopathy

Alexis I. Brinkerhoff

Assessment of the Role of Poly (ADP-Ribose) Polymerase in Drug-Induced Cardiomyopathy

by

Alexis I. Brinkerhoff

A thesis submitted in partial fulfillment
of the requirements for the degree of
Master of Science of Public Health
with a concentration in Toxicology and Risk Assessment
Department of Environmental and Occupational Health
College of Public Health
University of South Florida

Major Professor: Raymond D. Harbison, Ph.D.
Giffe T. Johnson, Ph.D.
Marie Bourgeois, Ph.D.

Date of Approval:
March 23, 2016

Keywords: Acrolein, Cardiomyocytes, Nitrogen Mustards, Poly (ADP-ribose) Polymerase

ACKNOWLEDGMENTS

I am taking this opportunity to thank the people who have offered continuous support towards completion of this thesis: my advisor and mentor, Dr. Raymond D. Harbison, for his endless guidance; my committee member and research advisor, Dr. Giffe T. Johnson, for relentless encouragement, brainstorm sessions, and input; and my committee member, Dr. Marie Bourgeois, for meticulous note keeping and encouragement. Throughout the laboratory process, Ph.D. candidate Jayme P. Coyle offered continuous dedication through his commitment to the Environmental and Occupational Health Cell Culture Laboratory. For all of their support, humor, constructive criticism, and encouragement throughout this process and all previous research endeavors, my parents Dr. William T. Brinkerhoff and Barbara A. Brinkerhoff, best friend and personal chef, John Singh, sister, Dr. Lauren B. Brinkerhoff, and brother, D.P.T. candidate Kyle W. Brinkerhoff, deserve acknowledgments as well. I am grateful to have the help and guidance of such inspirational professors, colleagues, and family members. Lastly, I would like to thank the University of South Florida and the College of Public Health for their financial, logistical, and technological support. All of these entities have placed a considerable amount of confidence and faith in me; thank-you.

TABLE OF CONTENTS

LIST OF FIGURES

ABSTRACT

Drug-induced cardiotoxicity has resulted in a thorough evaluation of patient doses, treatments, and rehabilitation. One of the most commonly prescribed chemotherapeutic agents is cyclophosphamide. The active metabolite, acrolein, is one of the most potent inducers of cardiomyopathy. In this study, research was conducted on the H9c2 (2-1) cardiomyocyte cell line derived from the embryonic myocardium of *rattus norvegicus* to assess its competency for evaluation of the change in poly (ADP-ribose) polymerase (PARP) activity. The application of this model to study the effects of acrolein on PARP activation was chosen as an ideal determinant of cell damage produced by nitrogen mustards. To verify the legitimacy of this model, cardiomyocytes were exposed to acrolein in varying concentrations and time durations with a subsequent protein concentration measurement determined through the BCA Protein Assay. After the normalization of samples through volume adjustments and verification of sufficient protein, other aliquots were subjected to a PARP Assay in order to measure PARP activity. PARP was activated at exposure concentrations of 75 μM in all trials, with an average detection of 0.00569 ± 0.001 mU/200ng protein. Other concentrations showed varying degrees of PARP activation, verifying the model's competency. PARP activation implies the potential use of this model for further research into targeted molecular therapy of PARP inhibition. Therefore, this model has the ability to be used as an assessment tool for the combined use of PARP inhibitors and chemotherapeutic agents; it can be useful for future research investigating the use and efficacy of PARP inhibitors in reducing drug-induced cardiotoxicity.

CHAPTER ONE

Introduction

Drug-Induced Cardiotoxicity

Drug-induced cardiotoxicity is one of the most pertinent concerns of drug development and regimens. This cardiac damage can manifest as cardiomyopathy, valvular disorders, arrhythmias, infarctions, and heart failure. One of the most important disorders is cardiomyopathy, which is the replacement of healthy cardiac tissue with scar tissue. This can create an enlargement of the heart (dilated cardiomyopathy, usually associated with left ventricular dysfunction, causing abnormal rhythms and contraction/relaxation forces), a thickening of cardiac muscle (hypertrophic cardiomyopathy, heart cannot pump blood effectively) or making the heart more rigid (restrictive cardiomyopathy, heart cannot expand properly) (McCartan et al., 2012). These conditions are very serious, as the accumulation of scar tissue results in decreased cardiac output and abnormal electrical rhythms (Yeh et al., 2004). The manifestation of these symptoms results in arrhythmias (atrial fibrillation, severe QT prolongation linked to ventricular tachycardia), valvular disorders, and heart failure. Cardiotoxicity risk may be increased in patients with confounding factors, such as atherosclerotic disease, obesity, hypertension, previous myocardial infarctions, and other major heart conditions. Other risk factors for heart problems include the rate of drug administration, age, gender, and radiation to the cardiac region (Shakir & Rasul, 2009; Kamezaki et al., 2005; Feenstra et al., 1999; Goldberg et al., 1986).

Induced cardiotoxicity can occur through a wide variety of drugs, including anti-inflammatory drugs, such as prednisone, immunomodulating agents, such as methotrexate, alkylating agents, such as cyclophosphamide, and beta blockers, which are currently being tested as an adjuvant therapeutic intervention for cancer patients (Feenstra et al., 1999). Initial results have shown beta blockers to engender a synergistic effect with chemotherapeutic agents for decreasing tumor metastasis and recurrence (Nagaraja et al., 2013; Pasquier et al., 2011). As this new role for beta blockers is further investigated, results indicating its potential role in heart failure must be acknowledged. The critical component of all of the aforementioned inducers of cardiotoxicity is that each subtype is commonly prescribed during chemotherapeutic regimens. This is a critical issue because this form of toxicity is induced by humans. Most of the drugs known to cause cardiotoxicity currently have existing alternatives on the market, thus rendering resultant cardiotoxicity preventable. Currently, there are no known anthracyclines or alternatives to cyclophosphamide that produce the same positive effects and yet completely eliminate the risk of drug-induced cardiomyopathy (Feenstra et al., 1999). Therefore, research conducted with the intention of finding ways to mitigate the cardiotoxic effects produced from these drugs is paramount for increasing the quality of life and attempting to achieve the optimum level of health and wellness for each patient.

One class of drugs that have been consistently linked to drug-induced cardiomyopathy is alkylating agents. Alkylating agents have a DNA alkylation mechanism of action. Effects can be seen through mispairing (guanine pairs to thymine instead of the normal G=C hydrogen bond), scission, and inter/intrastrand crosslinking (Preuss, 2015). Heart issues tend to linearly correspond to the cumulative dose of alkylating agents. In other words, as the dose increases, the magnitude and severity of heart problems increases. The best prediction for cyclophosphamide

induced acute cardiotoxicity is based on dose concentration, not the cumulative dose, which is reflected through the onset of heart failure shortly after drug administration (Yeh et al., 2004; Dow et al., 1993).

The incidence of myocardial failure ranges from 11.36%, with doses varying from 87±22 mg/kg/day to 174±34 mg/kg/day (Braverman et al., 1991), to 19% lethality, with doses of 180 mg/kg over four days (Gottdiener et al., 1981). However, cardiotoxicity may be attributed to the administered dose, the total cumulative dose, or can be completely independent of any dose analysis (Shakir & Rasul, 2009). Alkylating agents are unable to target cancerous cells, thus causing changes in the genetic material of healthy cells as well as malignant cells. This contributes to many of the stereotypical side effects of chemotherapy, including cardiotoxicity. The onset of negative side effects may occur immediately after treatment, or near the end of the patient's life. In addition, it is important to note that chemotherapeutic regimens often include multiple drugs. Combining multiple drugs with different toxicities and mechanisms of action can help to overcome the limited log kill hypothesis associated with individual drug treatment. The effects of this combination have been shown to decrease tumor mutation rate and the development of resistant tumor cell populations (Foo & Michor, 2015; Housman et al., 2014; McDermott et al., 2014). Most combination therapies are prescribed with the intention of changing resultant side effects and efficacy; by overlapping drugs with partial toxicities, near additive cytotoxic effects can be achieved with minimum peripheral damage. The combination can be given over intensive pulse courses in order to allow the patient more time to regenerate bone marrow, thus decreasing the risk of infection. A clinical remission for most tumor types results from the additive effect of an average of three different chemotherapeutic agents (Frei & Eder, 2003). For example, one of the most common adjuvant breast cancer chemotherapeutic

regimes includes 5-Florouracil, epirubicin, and cyclophosphamide, consisting of an S-phase cell cycle specific pyrimidine analog, an anthracycline, and an alkylating agent, respectively (Erselcan et al., 2000; Bergh et al., 1998). The combined action of these drugs results in eliminating cancerous cells remaining after surgery and has shown to increase the number of positive patient outcomes (Jamieson et al., 2014).

Often, chemotherapeutic regimens consist of more than three agents. For example, the most common regimen for Non-Hodgkin lymphoma includes Rituximab, cyclophosphamide, doxorubicin, vincristine, and prednisone, consisting of a monoclonal antibody, an alkylating agent, a topoisomerase inhibitor, a tubulin binder, and an anti-inflammatory agent, respectively (McCloskey et al., 2013; Luminari & Federico, 2011). This combination therapy, commonly known as R-CHOP, illustrates that multiple drugs with different mechanisms of action, targets, and toxicities confound the ability to directly correlate drug-induced cardiotoxic effects with one specific agent (King & Perry, 2001). However, severe toxicities, such as myocardial ischemia, still result (Federman & Henry, 1997). This type of ischemia-reperfusion is systemic and has been investigated for analysis of PARylation after this type of injury. This has resulted in research that investigates the role of PARP in global ischemia reperfusion *in vivo*, indicating the potential for PARP inhibitors to prevent myocardial dysfunction (Zhou et al., 2006; Fiorillo et al., 2002; Fiorillo et al., 2003). In addition to being administered as combination therapy, the dose administered is not always consistent (Brockstein et al., 2000; Nieto et al., 2000; Goldberg et al., 1986; Appelbaum, et al., 1976). As a result, it is often difficult to conclusively attribute heart conditions to a specific chemotherapeutic agent in the clinical setting. Thus, most of the existing literature connecting cardiotoxicity with specific chemotherapeutic drugs is associated with *in vitro* analyses (Inoue, et al., 2008). However, cardiotoxicity is consistently seen in

patients receiving cyclophosphamide treatment. Currently, the dose-limiting effect in therapeutic regimens containing cyclophosphamide is cardiotoxicity (Nishikawa et al., 2015).

Nitrogen Mustards

Nitrogen mustards are the most commonly prescribed alkylating agents (Colvin, 2003). These drugs are generally cell cycle nonspecific and directly act on DNA during all phases of the cell cycle, including the resting stage, in order to prevent replication (Fitzakerley, 2015). This is done mainly by cross-linking purine nucleobases between strands, thus preventing cell division (Bignold, 2006). This type of DNA damage induces cell death reflective of necrosis, *id est*, independent of apoptotic regulators (Zong, et al., 2004). In addition to damaging the DNA, these drugs also induce severe immunosuppression and damage the bone marrow. In addition, P450 mixed function oxidase enzymes catalyze reactions for drug metabolism and synthesis of lipids, proteins, cholesterol and steroids. Essentially these enzymes, in conjunction with oxygen and NADPH, induce polymorphisms to any xenobiotic substances which enter the body, creating polar metabolites. These result in deactivation (and thus drug elimination), hormone synthesis, or bioactivation. The latter can result in cancer chemotherapy or mutagenesis carcinogenesis (Anderson et al., 1995).

Cyclophosphamide is one of the most useful chemotherapeutic agents. It has been commonly prescribed to patients over the past forty years for a wide range of cancers and for kidney disease in children. It is a prodrug, and must be converted through the cytochrome P450 system and bioactivated post absorption after oral or intravenous administration in order to achieve cytostatic effects (C.S. Chen et al., 2004). Absorption by the body is faster with oral administration than with intravenous, which is reflected through peak plasma concentrations

occurring at 1.32 versus 5.97 hours (Juma et al., 1979). The active metabolites of cyclophosphamide are considerably more mutagenic and teratogenic than the drug itself (Hales, 1982). Bioactivation of the polar metabolites occurs primarily in the liver through CYP2A6, 3A4, 3A5, 2B6, 2C8, 2C9, 2C18 and 2C19 to form 4-hydroxycyclophosphamide (Helsby et al., 2010; Griskevicius et al., 2003; Huang et al., 2000). This product, existing in equilibrium with its tautomer aldophosphamide, is heavily favored in this reaction (Nishikawa et al., 2015; Moore, 1991). Another transformation, albeit less favored, occurs through CYP3A4, 2B6, and 3A5 in order to form chloro-acetaldehyde and 2-dechloroethyl cyclophosphamide (Makowski, 2015). The products from the favored reaction are further oxidized to form carboxycyclophosphamide. However, this final reaction is not driven to completion and the remaining aldophosphamide diffuses into cells where it is cleaved to the active metabolites carboxyethylphosphoramide mustard and acrolein (Micetich, 2014; Hardman et al., 1996). Both of these metabolites and up to 25% of the parent compound are eventually eliminated from the body (Tomita et al., 2004).

Acrolein (C_3H_4O), the simplest unsaturated aldehyde, is created endogenously as an active metabolite of multiple nitrogen mustards, the most notable being cyclophosphamide. Acrolein reacts with nucleophilic sites, including protein thiol moieties through addition and Schiff base formation (ATSDR, 2007). It is highly reactive, forming acrolein-thiol conjugates and actively inhibiting aldehyde dehydrogenase-1 (Ren et al., 1999; Bunting & Townsend, 1998). It is highly unstable and volatile at standard temperature and pressure, readily reacting via polymerization with oxidizing agents (Arntz et al., 2012; LoPachin, et al., 2009). In order to minimize these effects, acrolein is stabilized with the reducing agent hydroquinone, $C_6H_6O_2$ (Parry, 1948). Therefore, simultaneous exposure of cardiomyocytes to hydroquinone was performed to detect potential direct and indirect data interferences. The chosen concentrations of

acrolein and hydroquinone were decided based on *in vitro* experimental observation and prediction for clinical relevancy. Normal doses of intermittent cyclophosphamide therapy are administered intravenously at 40-50 mg/kg/day (400-1800 mg/m^2) over a period of two to five days; for continuous daily therapy, doses normally range from 1-2.5 mg/kg/day; during the R-CHOP regimen, cyclophosphamide is given intravenously at 400-1500 mg/m^2 for each day of the treatment (US FDA, 1959). As with all chemotherapeutic regimens, the dosage may be adjusted based on the patient's individualized response. The concentrations chosen for this research experiment were translated from the higher clinical exposures and encompass exposure concentrations much higher than prescribed in the clinical setting (e.g., 125µM). However, these acrolein concentrations are commonly seen in patients with Alzheimer's disease and in patients with renal failure. In this latter situation, the inability of the kidneys to filter out the acrolein results in its high sequestering. Accumulated protein-bound acrolein has been measured up to 180µM in patients with renal failure (Sakata et al., 2003). This accretion of acrolein allows a somewhat surjective function between laboratory and clinical experimentation to be formed. In other words, the laboratory exposures, ranging from 50-125µM, can be observed in the clinical setting.

Acrolein induces p53 activation and apoptosis in human alveolar macrophages, keratinocytes, and bronchial epithelial cells via induction of the mitochondrial pathway (Roy et al., 2010; Tanel & Averill-Bates, 2005). TP53 tumor suppressor gene activation, leading to increased p53 protein production, results in cell cycle arrest and failure to permit DNA repair. Premature aging and cell degradation results from p53 accumulation (Nicolai et al., 2015). One of the most severe disorders associated with acrolein toxicity is hemorrhagic necrosis. This is commonly associated with high-dose regimens of cyclophosphamide and is often fatal

(Katayama et al., 2009). Acute, high-dose regimens limit immune responses through NFκB suppression, which increases patient risk for secondary infections (Horton et al., 1999). On the other hand, chronic, low- to average-dose regimens have been associated with enhanced inflammatory responses, such as those observed induced by NFκB, which leads to inflammation and injury (Moghe et al., 2015). Observed in the heart, this can result in myocarditis. However, low-dose regimens have been shown to engender adaptive effects against future doses received at higher concentrations (Sthijns et al., 2014). This could prove beneficial for patients receiving chronic treatments and should be investigated further with respect to potential drug regimens.

Due to the difficulty of maintaining and the fragility of primary cardiomyocytes in culture, in conjunction with ethical concerns relative to animal studies, the H9c2(2-1) cardio myoblast cell line was implemented. This line is a subclone of the cell line derived from BDIX *rattus norvegicus* by Kimes & Brandt (1976). Since then, this embryonic line has been thoroughly researched and continues to be utilized throughout biochemical, pharmacological, and electrophysiological research (Hescheler et al., 1991). An imperative characteristic of this line is its ability to retain elements of signaling pathways existing in cardiac cells, such as differentiating to myotubes and retaining a cardiac muscle phenotype (Branco et al., 2015; Sardão et al., 2007; van der Putten et al., 2002; Menard et al., 1999). In addition, these cells have been shown to respond similarly to hypertrophic responses seen in primary cardiomyocytes (Watkins et al., 2011). Recently, the H9c2(2-1) line has been used to investigate cyclooxygenase inhibitors (Sakane et al., 2014), the interactions between PARP-1 and the RNF146 (ring finger protein 146) gene (Gerö et al., 2014), anthracyclines (Studzian et al., 2015), nitrogen mustards (Nakamura et al. 2010), flavonoids (Chen et al., 2014), and many other things. This model continues to be highly regarded and implemented in the research setting.

Poly (ADP-Ribose) Polymerase

Poly(ADP-Ribose) polymerase (PARP) is a subfamily of 17 cell signaling enzymes which greatly influence genomic stability, metabolic processes at the cellular level, cell replication, and cell death (Otto et al., 2005; Hassa & Hottiger, 2008). Each of these enzymes are comprised of four main domains: N-terminal DNA binding, ADP-ribosylating catalytic, caspase-cleaved, and auto-modification (Kow & Doetsch, 2005). The N-terminal DNA binding domain is comprised of two zinc fingers which systematically identify DNA discontinuities. These can bind to an allosteric site on the DNA, thus initiating single-strand break (SSB) or double-strand break (DSB) repair pathways (Ahel et al., 2008; Ikejima et al., 1990). In most cases, this induces the formation of PAR chains (hydrolyzed by poly (ADP-ribose) glycohydrolase), which rapidly consumes NAD^+ and ATP, producing nicotinamide in the process termed PARylation (Reviewed in Amé et al., 2004). This nicotinamide acts to reversibly inhibit PARP through a negative feedback loop. Stability of intracellular NAD^+ and ATP levels is also sustained through competition for free NAD^+. This is extremely important in preventing excess NAD^+ and ATP depletion which can lead to cell lysis and necrosis through decreased glycolysis and mitochondrial respiration (De Vos et al., 2012). This can be seen through competition between the tumor suppressor sirtuin-1 and PARP-1 (Kolthur-Seetharam et al., 2006). Sirtuin-1 also acts to inhibit E2F-1, whose expression is otherwise controlled by PARP-1 (Nogueiras et al., 2012). The catalytic domain contains a BRCA1 C-terminus motif and auto-PARP sites, which are associated with PARP catalytic activities, such as NAD^+ hydrolysis and its cascading effects. This domain serves to link the family members with respect to phylogeny (Perina et al., 2014). This unique catalytic motif serves as an exclusion mechanism for members of the PARP family: if the domain is present, they are included in the superfamily regardless of DNA binding

capabilities (Swindall et al., 2013). The caspase-cleaved domain is responsible for caspase-9 and caspase-3 mediated cleavage, which plays an important role in the type of cell death that occurs (De Vos et al., 2012). The auto-modification domain contains the BRCA1 C-terminus (BRCT) domain, which limits enzyme activation through its regulation of hetero-ADP-ribosylation and has been linked to the interactions between PARP and DNA (Drew, 2015; D'Amours et al., 1999; Kameshita et al., 1984).

Out of all the different family members, PARP-1 (with a molecular weight of 116 kDa) has been subjected to the most research due to its proliferation, regulation of transcription, modification to chromosome structure and function, and cellular signaling (Wacker et al., 2007; Monaco et al., 2005). The catalytic activity of PARP-1 is located at the carboxy-terminal region (Swindall et al., 2013; Eustermann et al., 2011) and its basal activity is irrespective of DNA damage (Kow & Doetsch, 2005). PARP-1 DNA repair commences with early recognition and subsequent bending of the nicked region. Permitted by the sugar-phosphate backbone gap, this bending (approximately 100°) enables the correct repair method to be chosen based on nick physiognomies (Kow & Doetsch, 2005). These repair methods most commonly consist of base excision repair, SSB repair, and DSB repair through non-homologous end joining and subsequent homologous recombination (Beck et al., 2014; Saberi et al., 2007; Frank-Vaillant & Marcand, 2002).

Catalytic activity of PARP-1 is controlled by the auto-modification BRCT domain described above, in addition to a WGR amino acid domain (so named for the amino acid residues tryptophan (W), glycine (G), and arginine(R)), which has been shown to offer protective effects from oxidative stress *in vitro* (Li et al., 2014; Altmeyer et al., 2009). The location and composition of the BRCT and WGR domains allows PARP-1 to be phylogenetically

distinguished from the other family members (Daugherty et al., 2014; Ruf et al., 1998). The PARylation PARP-1 undergoes with DNA binding results in its ability to regulate p53 and RNA polymerases I and II (Swindall et al., 2013). In addition, PARP-1 controls transcription through direct regulation of the aP2, Cox-2, E2F-1, and Oct1 transcription factors (Erener et al., 2011; Lin et al., 2011; Nie et al., 1998). These transcription factors are important in promoting gene expression relevant to DNA replication and cell growth (e.g., the pRb protein acts as a cell cycle checkpoint for E2F-1) (Simbulan-Rosenthal et al., 2003). In some instances, PARP-1 can change the function of transcription factors. For example, this occurs in NFκB, where PARP-1 directly interacts with p50 and p63 subunits in order to modify protein function (Kameoka et al., 2000). This change to NFκB protein function prevents the activation of immune responses such as inflammation (Petrilli et al., 2004). With all of these influential characteristics, PARP-1 has a clear upstream effect on cell regulation.

PARP-1 impacts three main forms of cell death: necrosis, parthanatos, and apoptosis. Necrotic cell death is mediated by PARP-1 activation of JNK (c-Jun N-terminal kinase), most notably JNK1, which induces large-scale DNA cleavage and fragmentation (Xu et al., 2006). It is important to note that TNF (tumor necrosis factor)-induced necrosis is now considered independent of the PARP pathway due to the fact that inhibition of PARP-1 prevents the activation of the PARP pathway by methyl methanesulfonate, but fails to prevent TNF-induced necroptosis. In addition, interference with ceramide generation or the function of receptor-interacting proteins still results in necrosis through the PARP pathway, yet it obstructs TNF-induced necrosis (Sosna et al., 2014). When severe oxidative stress occurs, PARP-1 initiates poly(ADP-ribosyl) formation which induces translocation of cytochrome *c* and AIF (mitochondrial apoptosis-inducing factor) to the nucleus. Translocation causes DNA cleavage

and fragmentation, eventually resulting in parthanatos (PARP-1 mediated cell death) or apoptosis (Andrabi et al., 2006). Parthanatos and apoptosis are very similar and display the same form of AIF translocation and caspase-3 mediated cleavage (albeit late activation with parthanatos); however, their distinct causes (parthanatos from excess PAR and apoptosis from cell signaling) distinguish between the two (Fatokun et al., 2014). It has been demonstrated in cardiomyocytes that cytochrome *c* and AIF translocation induced by oxidative stress can be decreased with PARP inhibitors through mitochondrial transmembrane potential reduction (M. Chen et al., 2004).

The Role of PARP in Acrolein-Induced Cardiomyopathy

Inhibiting PARP may reduce toxic effects and offer protection against cytotoxicity and apoptosis, which has been suggested in numerous studies (Conklin et al., 2015; Samol et al., 2011; Tanel & Averill-Bates, 2007; Szabó, 2005; Hall, 1980). The relationship between PARP-1 and apoptosis, most notably the change in mitochondrial function, causes increased intracellular sodium and calcium levels which contributes to cardiomyopathy and other heart ailments (Szabó, 2005). The application of PARP inhibitors can attenuate the mitochondrial injury associated with nitrogen mustards, thereby conserving energy and preserving myocardial function (Virág et al., 1998; Satoh et al. 1994). In addition to generically decreasing toxicities, PARP inhibitors have also been associated with eliminating negative effects related to cardiac reperfusion (Reviewed in Jagtap & Szabó, 2005; Szabó, 2005). In a cardiac reperfusion study on isolated rat hearts conducted by Yamazaki and associates (2004), the PARP inhibitor 3-aminobenzamide was able to improve heart function by suppressing oxidative stress. These cardioprotective effects of

PARP inhibitors validates continued research in order to discover the potential these enzyme inhibitors have in therapeutic interventions.

Purpose

Acrolein induces apoptosis via activation of the mitochondrial pathway and has been shown to produce DNA damage *in vivo,* leading to multiple ailments including cardiomyopathy (Ismahil et al., 2011; Luo et al., 2007; Uchida et al., 1998). PARP is involved in apoptosis, and PARP inhibition has been shown to offset oxidative damage (Lupo & Trusolino, 2014; Eliasson et al., 1997; Zhang et al., 1994). As a result, the H9c2 (2-1) cardiomyocyte cell line was investigated as a potential model for further examination of acrolein-mediated cardiomyopathy. In order to help elucidate the role of PARP in acrolein-induced cell toxicity, this research was conducted. Consistent with contemporary literature, the H9c2 (2-1) cardiomyocyte cell line should form a competent model for evaluation of PARP activation from acrolein exposure (Roy et al., 2010; Conklin et al., 2015; Dong et al., 2013; Tanel & Averill-Bates, 2005).

CHAPTER TWO

Methods

This study was divided into two main sections: the first (initial time trial) was conducted with an aim of determining an appropriate exposure duration for optimum testing of the cardiomyocytes; the second (trials 1-3) was conducted using refined methods for obtaining trial data.

Cell Culture

This experiment was conducted *in vitro* using embryonic myocardium from *rattus norvegicus*, cell line H9c2 (2-1). This cell line was chosen due to its ability for continued propagation and its relevance to cardiotoxicity. The line itself was obtained from the American Type Culture Collect (ATCC) (CRL-1446; Manassas, VA) and arrived in the Environmental and Occupational Health Cell Culture Laboratory (Tampa, FL) in February 2015. The line was cultured in a humidified atmosphere of 5% CO_2 at 37°C. Complete supplemented medium was created with Debulcco's Modified Essential Medium (Corning, Manassas, VA) from a mixture of HEPES buffer (Sigma, St. Louis, MO), fetal bovine serum (ATCC), and penicillin-streptomycin (ATCC) prior to use (see appendix 1). Complete supplemented medium was stored in a sterilized 4°C environment until it was needed for culturing plated cells or for diluent purposes. This process of complete DMEM media use was continued until approximately 0.75 inches of solution remained. At this point, the remaining solution was discarded and new

complete supplemented medium was created to reduce contamination and degradation. In addition to this change in complete DMEM media, supplemented media used for culturing cells was changed roughly every other day. At 85-90% confluence, approximately every five days, cardiomyocytes were disaggregated with 0.1% Trypsin EDTA in PBS (Corning, Manassas, VA) (see appendix 2). The supernatant resulting from warm trypsinization was either frozen for long-term storage (rate-controlled), reconstituted in supplemented DMEM and plated out for directed experimentation, or split at a subcultivation ratio of 1:4 and plated for further propagation. If reconstituted for experimentation, the cell concentration and viability was evaluated prior to plating through trypan blue dye exclusion viability assessment (Lonza Cologne GmbH, 2012). For this procedure, cells underwent trypsinization and were reconstituted with supplemented DMEM (see appendix 2). An aliquot of the re-suspended cell solution was combined with trypan blue (0.1% trypan blue in DPBS; Corning) in a 1:1 ratio. The number of cells and viability was evaluated with the use of a hemocytometer.

The line underwent eleven passages before exposure to acrolein commenced. As cells are subject to morphological changes with each passage, it is important to note that cell shape changes did not naturally occur as of passage fourteen. However, complete omission of natural changes cannot be ruled out; as of passage fourteen, cells had started forming domes, indicative of loss of contact inhibition and cell differentiation. Exposure to acrolein occurred only after cells were given adequate time to reattach to the plates. Acrolein exposure resulted in morphological changes: mainly the cell structure changed from a long fusiform shape to a multinucleated, condensed spherical shape.

Cell Treatment

For all trials, cells were counted and viability was assessed using trypan blue exclusion with the use of a hemocytometer prior to plating for experimentation. For the initial time trial, H9c2 (2-1) cells were plated in three 6-well plates (Corning) at approximately 100,000 cells per well and allowed to attach over a 36 hour time span. For trials 1-3, cardiomyocytes were plated in 24-well plates (Celltreat, MA) at approximately 100,000 cells per well and permitted 36 hours to attach. Prior to acrolein exposure, 10X PARP buffer was mixed and then used in the mixture of lysis buffer (see appendix 4 and 5); 0.3% hydroquinone solution was created with 0.3% hydroquinone (Sigma, St. Louis, MO) and ddH_2O in a ratio of 1:1 until appropriate volumes were achieved; inert conditions were prepped. Upon receiving acrolein (Sigma-Aldrich, St. Louis, MO) under inert conditions, its density was calculated in order to ensure appropriate volumes for dilution. This was done by extracting 100µL from under inert conditions, weighing the acrolein under sterile conditions, and applying basic algebra (by using the equation density=[mass/volume]). The density was used to calculate its molarity and the appropriate dilution volumes were determined by applying basic algebra (by using the equation $C_1V_1 = C_2V_2$, where C_1 is the concentration of acrolein received from Sigma-Aldrich, V_1 is the unknown variable which will be the volume of acrolein necessary for desired dilution, C_2 is the desired concentration, and V_2 is the desired volume). Acrolein was extracted and homogenized with ddH_2O in a 1:1000 ratio to ensure that the correct amount from the density calculation (2.157×10^{-4} µL) was obtained (Newton, 1991; EPA, 2015). Cells then underwent the exposure procedure: both the 0.3% hydroquinone solution and acrolein solution underwent serial dilutions; supplemented medium was aspirated and subsequently followed with a PBS wash and the addition of the appropriate concentration (50-125 µM) of the control (0.3% hydroquinone in

completely supplemented DMEM) or the treatment (acrolein in completely supplemented DMEM).

For the initial time trial, plates were incubated corresponding to their appropriate exposure duration (three plates: one with an exposure duration of 25 minutes, one with an exposure duration of 55 minutes, and one with an exposure duration of 75 minutes). These cells were all exposed to either 75µM of 0.3% hydroquinone or 75µM of acrolein. For trials 1-3, cells were exposed to varying concentrations ranging from 50-125µM of 0.3% hydroquinone or acrolein and incubated for 55 minutes (see appendix 3). During the incubation, the remaining steps (addition of PMSF and DTT) of lysis buffer creation were completed. After the appropriate exposure duration was reached, cells were removed from the incubator, waste was aspirated, and 75µL lysis buffer was added to each well. Cell lysates were extracted and divided into two aliquots, one for protein quantification and one for the PARP assay. A minimal amount of residue was left upon recovery of cell lysates from the treated plates. Assessment of protein concentrations was conducted on one subgroup of lysates, a blank, and a lysis buffer control. The second subgroup of cell lysates was stored per manufacturer's instructions at -80°C until the PARP assay could be conducted.

Protein Quantification via BCA Protein Assay

In order to evaluate PARP activation, protein concentrations must be determined to adequately prepare the samples for the PARP assay. In order to determine protein concentrations, protein quantification was simultaneously run in duplicates on bovine serum albumin (BSA) protein standards and samples, according to the Pierce BCA colorimetric kit's (Pierce, Rockford, IL) manufacturer instructions (see appendix 4). The amount of protein detected was determined

via spectrophotometer (BioTek μQuant) exposure to 562 nm averaged across samples with similar expected concentrations. A standard polynomial was derived from the BSA protein standards and appropriate calculations were made to account for dilutions and protein present in the lysis buffer control. The final number was used to normalize the samples for the PARP assay by permitting determination of the volume of sample and the volume of PARP buffer diluent needed for each well during the PARP assay. Samples that produced insufficient protein (see results section) were not subjected to the PARP assay.

Poly (ADP-Ribose) Polymerase Assay

Colorimetric poly (ADP-ribose) polymerase assays quantify the inclusion of biotinylated PARP onto histone proteins. It is often used to assess DNA damage and to determine whether DNA damage was attributed to non-apoptotic cells. In this study, its use was intended for the measurement of PARP-1 activity in cell lysates. The second subgroup of cell lysates, previously stored at -80°C, were used to assess the amount of PARP-1 activity produced from treatment. This assay was run in triplicates on 96-well high-binding spectra plates (Perkin Elmer) with PARP HSA standards simultaneously run for each plate. The PARP colorimetric assay kit used was a modification from that produced by Trevigen in 2013 in order to decrease overall costs (see appendix 5). This modification was previously verified within appropriate statistical significance and validated for cell culture use. This assay was comprised of three main sections, relative to the day on which they were performed: histone plating, blocking step, and detection. The PARP assay culminated in the determination of PARP activity measured via spectrophotometer at an exposure of 450 nm and averaged across samples with similar concentrations and treatment methods.

CHAPTER THREE

Results

The initial trial was conducted with the goal of determining an appropriate exposure duration before treatment with different concentrations of acrolein. In the initial trial, trypan blue exclusion assessment showed that the cells were 95.33% viable.

Protein Quantification Results from Initial Time Trial

Cardiomyocytes were treated with 75μM acrolein and protein quantification was run on lysates to detect protein concentrations and ensure the appropriate use of the PARP assay. Standard concentrations of bovine serum albumin were run simultaneously to the samples. The standard curve for the BCA protein quantification assay produced an R^2 value of 0.997. As depicted in Figure 1, an exposure duration of twenty-five minutes produced an average concentration of 1,479.362±599 μg/mL; an exposure duration of fifty-five minutes produced an average concentration of 911.474±275.558 μg/mL; an exposure duration of seventy-five minutes produced an average concentration of 883.161±161.495 μg/mL. All averages were blanked against the lysis buffer control of 2277±112.544 μg/mL to account for possible interference. The aliquots from each well produced sufficient protein measured in the protein quantification assay to permit an effective PARP assay to be run on the replicates. Appropriate sample dilutions for the PARP assay were determined from the detected protein concentrations.

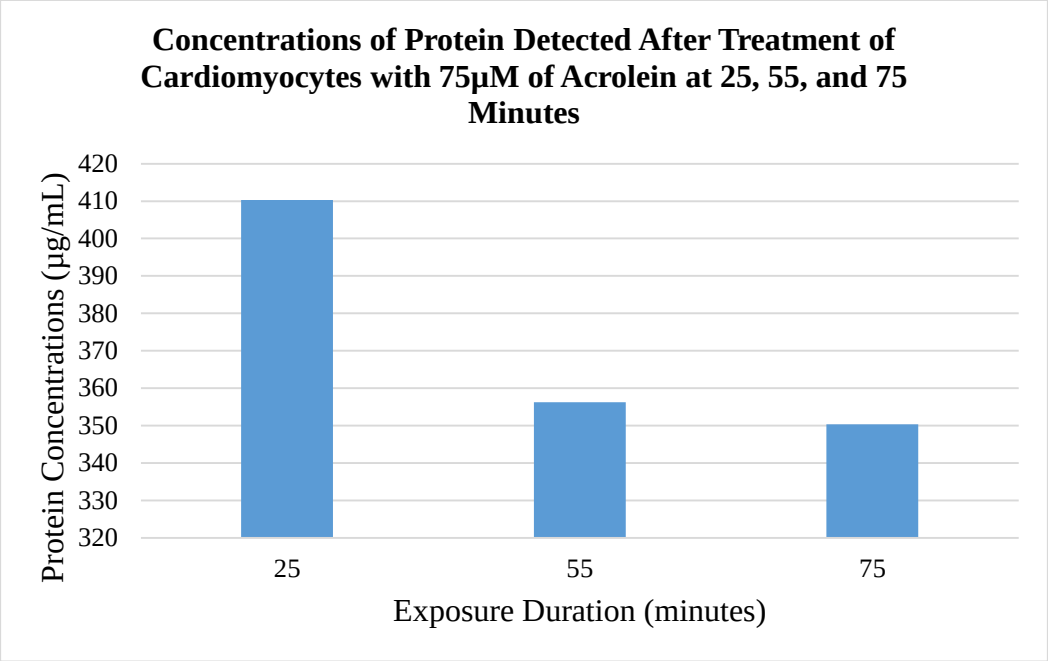

Figure 1: Concentrations of protein detected after treatment of cardiomyocytes with 75µM acrolein at 25, 55, and 75 minutes. There is a weak trend depicting increased protein concentration with decreased exposure duration.

PARP Activity Detection Results from Initial Time Trial

PARP activity detection upon cardiomyocyte exposure to 75µM acrolein were clustered with an absorbance around 0.3 micro unit of PARP activity per 200 ng of protein (per well). As shown in Figure 2, an exposure duration of twenty-five minutes produced an average PARP activity detection of 0.26±0.064 µU/200ng protein; an exposure duration of fifty-five minutes produced an average of 0.348±0.199 µU/200ng protein; an exposure duration of seventy-five minutes produced an average of 0.299±0.071 µU/200ng protein. The line of best fit assumed a polynomial of order two, producing an R^2 value close to 1. All averages were blanked against the lysis buffer control in order to account for possible interference. The standard curve for the PARP assay for quantification of values against known PARP enzyme concentrations (not shown) produced an R^2 value of 0.994.

Despite the result's standard deviation of 0.199, an exposure duration of fifty-five minutes was chosen due to the highest detection irrespective of standard deviation, detection above the control, and its consistency with the literature (Roy et al., 2009). Acrolein exposure of cardiomyocytes was chosen to be given in concentrations of 50 μM, 75 μM, 100 μM, and 125μM based primarily on a literature review, with exposures around 100 μM producing the most consistent results (Wang et al., 2011; Luo et al., 2007; Kehrer et al., 2000).

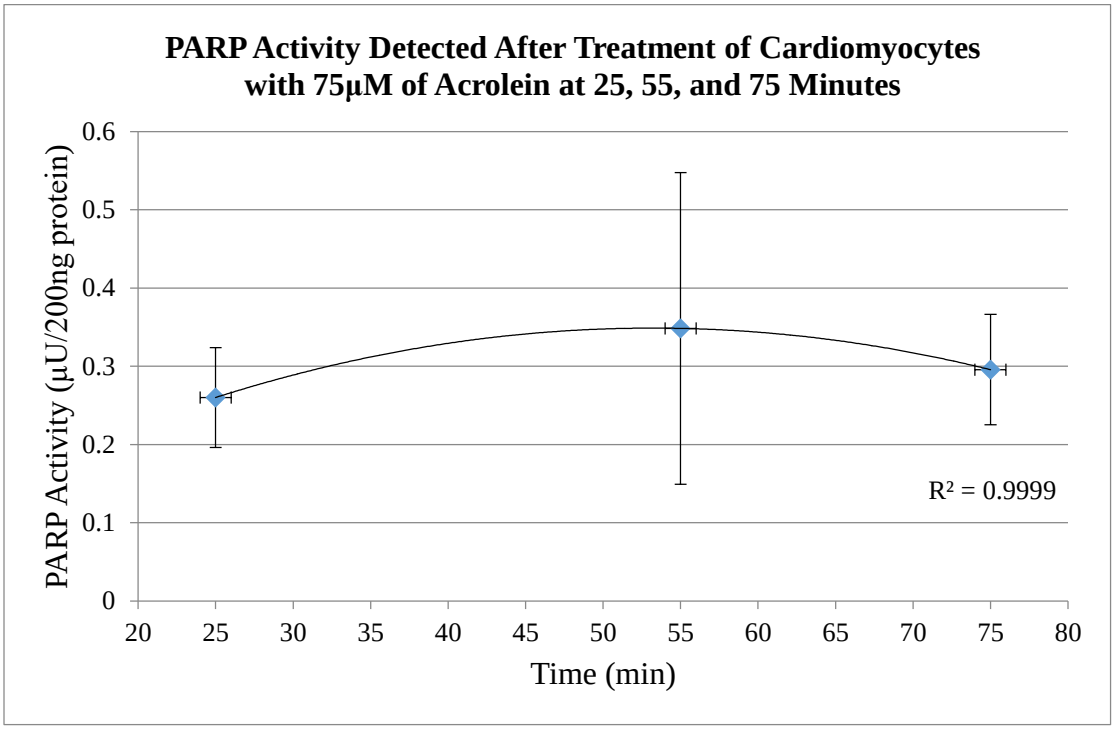

Figure 2: PARP activity detected after treatment of cardiomyocytes with 75μM of acrolein at 25, 55, and 75 minutes. Time of 25 mins produced an average detection of 0.26±0.064, a time of 55 mins produced an average detection of 0.348±0.199, and a ime of 75 mins produced an average detection of 0.299±0.071, with all units in micro units of PARP activity per 200ng of protein.

Trials 1, 2, and 3 were conducted to evaluate PARP activity upon treatment of cardiomyocytes with different acrolein concentrations for an exposure duration of fifty-five minutes. Trypan blue exclusion cytotoxicity assessment showed that cell viability was 96.15%, 93.67%, and 96.01% for trials 1, 2, and 3, respectively. In these trials, cardiomyocytes were

treated with varying acrolein concentrations and protein quantification was run on lysates on 96-well plates in duplicates to ensure appropriate protein concentrations existed to run the PARP assay. Standard concentrations of bovine serum albumin were run in duplicates simultaneously to the samples for each plate.

Protein Quantification Results from Trial 1

Protein quantification of samples from trial one was run in duplicates on two 96-well plates. The standard curve for the BCA protein quantification assay from plate 1 produced an R^2 value of 1 (rounded up from 0.9999). The standard curve for the BCA protein quantification assay from plate 2 produced an R^2 value of 0.999. The aliquots from each well produced sufficient protein in the protein quantification assay to permit an effective PARP assay to be run on the replicates after proper dilutions.

As depicted in Figure 3, an acrolein concentration of 50μM produced an average protein concentration of 246.885±63.631 μg/mL, whereas the hydroquinone concentration of 50 μM produced an average concentration of 332±78 μg/mL; an acrolein concentration of 75 μM produced an average protein concentration of 387±243 μg/mL, whereas the hydroquinone concentration of 75 μM produced an average concentration of 908±318 μg/mL; an acrolein concentration of 100 μM produced an average protein concentration of 764±149 μg/mL, whereas the hydroquinone concentration of 100 μM produced an average concentration of 1262±407 μg/mL; an acrolein concentration of 125 μM produced an average protein concentration of 1051±404μg/mL, whereas the hydroquinone concentration of 125 μM produced an average concentration of 1111±418 μg/mL.

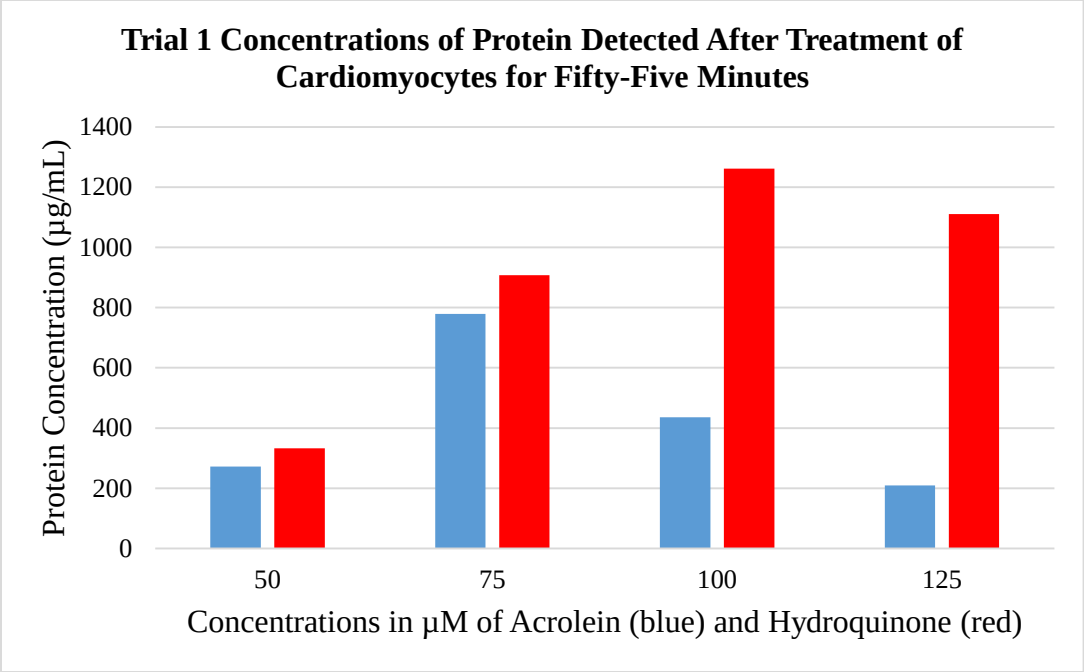

Figure 3: Trial 1 concentrations of protein detected after treatment of cardiomyocytes for fifty-five minutes. Cells treated with 50 µM, 75 µM, 100 µM, and 125 µM of acrolein (blue) and hydroquinone (red). When blanked against the lysis buffer control, the resulting protein concentrations show increasing protein concentration with increasing exposure.

Protein Quantification Results from Trial 2

Protein quantification of samples from trial two was run in duplicates on two 96-well plates. The standard curve for the BCA protein quantification assay from plate 1 produced an R^2 value of 1 (rounded up from 0.9999). The standard curve for the BCA protein quantification assay from plate 2 produced an R^2 value of 0.990. The results from this assay were more inconsistent than those produced from trial 1, as insufficient protein was detected after blanking against the corresponding lysis buffer control in four of the acrolein-exposed wells (accounting for 16.67% of the acrolein-exposed wells and 3.03 % of the total number of wells) and four of the hydroquinone-exposed wells (accounting for 16.67% of the hydroquinone-exposed wells and 3.03% of the total number of wells). As these wells produced insufficient protein, corresponding

aliquots were not used for PARP detection testing. These wells were disregarded in the calculation of average protein concentrations shown in Figure 4.

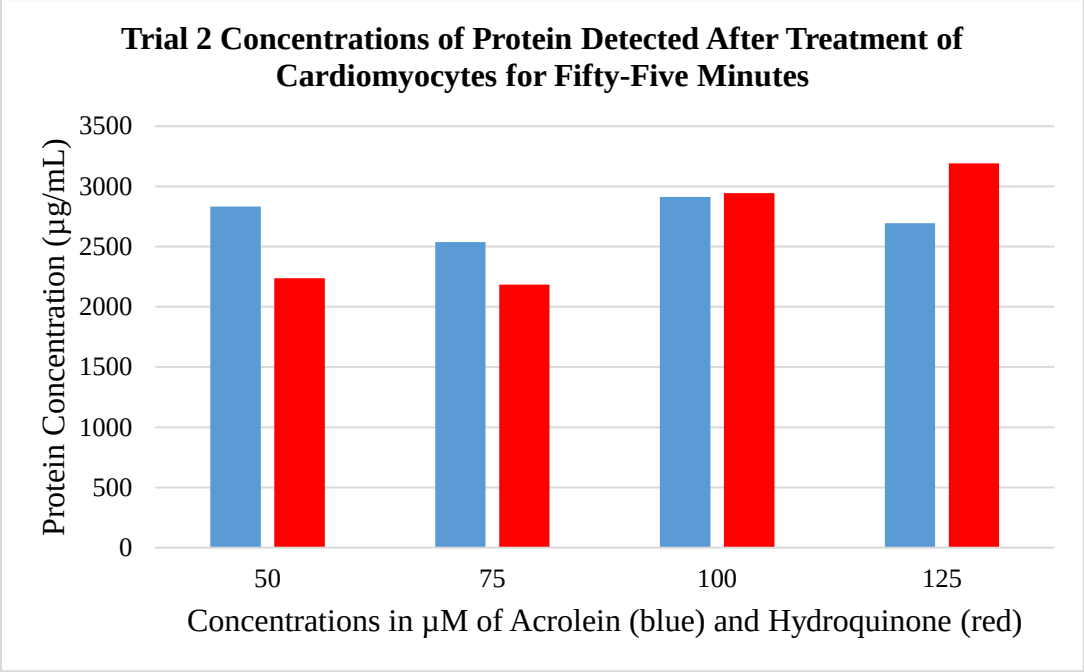

Figure 4: Trial 2 concentrations of protein detected after treatment of cardiomyocytes for fifty-five minutes. Cells treated with 50 µM, 75 µM, 100 µM, and 125 µM of acrolein (blue) and hydroquinone (red). When blanked against the lysis buffer control, the resulting protein concentrations show no significant correlations with exposure concentrations.

As depicted in Figure 4, when blanked against the lysis buffer control, an acrolein concentration of 50 µM produced an average protein concentration of 2832 ±169 µg/mL, whereas the hydroquinone concentration of 50 µM produced an average concentration of 2238±302 µg/mL; an acrolein concentration of 75 µM produced an average protein concentration of 2536±304 µg/mL, whereas the hydroquinone concentration of 75 µM produced an average concentration of 2183±517µg/mL; an acrolein concentration of 100 µM produced an average protein concentration of 2912±678 µg/mL, whereas the hydroquinone concentration of 100 µM produced an average concentration of 2944±815 µg/mL; an acrolein concentration of 125 µM

produced an average protein concentration of 2693±122 µg/mL, whereas the hydroquinone concentration of 125 µM produced an average concentration of 3190±705 µg/mL.

Protein Quantification Results from Trial 3

Protein quantification of samples from trial three was run in duplicates on two 96-well plates. The standard curve for the BCA protein quantification assay from plate 1, corresponding to the lower concentrations, produced an R^2 value of 0.999. The standard curve for the BCA protein quantification assay from plate 2, corresponding to higher concentrations, produced an R^2 value of 0.997. The results from this assay were more inconsistent than those produced from trial one, but less inconsistent than trial two, as insufficient protein was detected after blanking against the corresponding lysis buffer control in three of the acrolein-exposed wells (accounting for 12.5% of the acrolein-exposed wells and 2.14% of the total number of wells) and two of the hydroquinone-exposed wells (accounting for 8.33% of the hydroquinone-exposed wells and 1.43% of the total number of wells). As these wells produced insufficient protein, corresponding aliquots were not used for PARP detection testing. These wells were disregarded in the calculation of average protein concentrations shown in Figure 5. As depicted in Figure 5, when blanked against the lysis buffer control, an acrolein concentration of 50 µM produced an average protein concentration of 515±350 µg/mL, whereas the hydroquinone concentration of 50 µM produced an average concentration of 380±171 µg/mL; an acrolein concentration of 75 µM produced an average protein concentration of 279±142 µg/mL, whereas the hydroquinone concentration of 75 µM produced an average concentration of 259±151 µg/mL; an acrolein concentration of 100 µM produced an average protein concentration of 605±303 µg/mL, whereas the hydroquinone concentration of 100 µM produced an average concentration of

613±203µg/mL; an acrolein concentration of 125 µM produced an average protein concentration of 805±247 µg/mL, whereas the hydroquinone concentration of 125 µM produced an average concentration of 858±333 µg/mL.

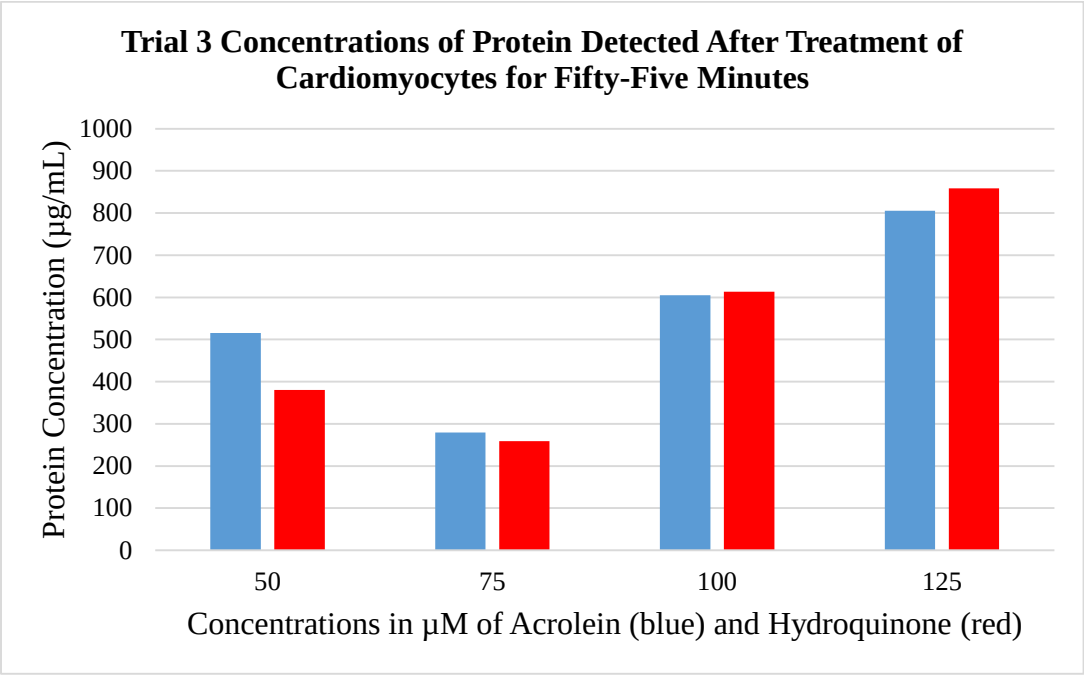

Figure 5: Trial 3 concentrations of protein detected after treatment of cardiomyocytes for fifty-five minutes. Cells treated with 50 µM, 75 µM, 100 µM, and 125 µM of acrolein (blue) and hydroquinone (red). When blanked against the lysis buffer control, the resulting protein concentrations show no significant correlations with exposure concentrations. The protein concentrations from cells treated with acrolein are similar to the protein concentrations from cells treated with hydroquinone.

PARP Activity Detection Results from Trials 1 and 2

PARP activity detection upon cardiomyocyte exposure to varying acrolein concentrations varied significantly. This PARP assay was run in triplicates on aliquots collected from trials one and two and it required the use of three different plates. The standard curve for this PARP assay for plate one produced an R^2 value of 0.996, the standard curve for plate two had an R^2 value of 0.985, and the standard curve for plate three produced an R^2 value of 0.996. For Figure 6, the R^2

value for the polynomial line of best fit was 0.0921, indicative that absorbance measurements cannot be precisely predicted through the acrolein exposure concentration. As illustrated in Figure 6, an acrolein concentration of 50 µM over an exposure duration of fifty-five minutes produced an average PARP activity detection of 0.000402±0.001 µU/200ng protein; an exposure over fifty-five minutes to an acrolein concentration of 75 µM produced an average PARP activity of 0.00736±0.0004 µU/200ng protein; an acrolein concentration of 100 µM produced an average of -0.00521±0.002 µU/200ng protein for an exposure duration of fifty-five minutes; an exposure duration of fifty-five minutes to an acrolein concentration of 125 µM produced an average PARP activity detection of 0.00648±.006 µU/200ng protein. All averages were blanked against the lysis buffer control on its corresponding plate in order to account for possible interference.

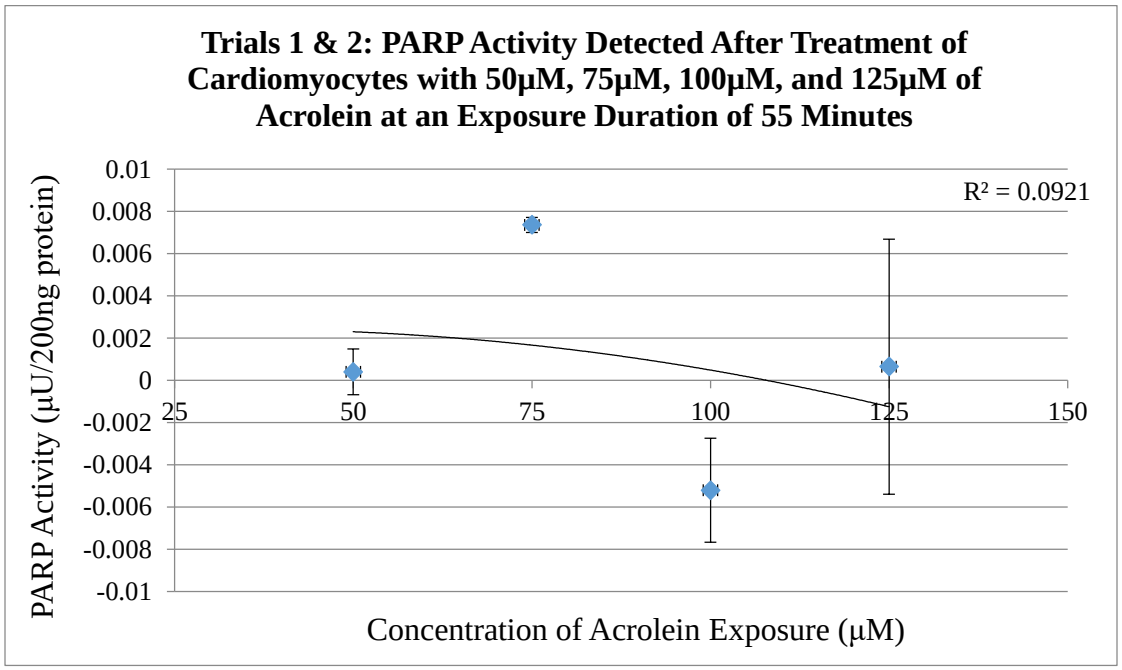

Figure 6: Trials 1 & 2: PARP activity detected after treatment of cardiomyocytes with 50 µM, 75 µM, 100 µM, and 125 µM of acrolein at an exposure duration of 55 minutes. Acrolein concentrations of (a) 50 µM produced an average of 0.000402±0.001; (b) 75 µM produced an average of 0.00736±0.0004; (c) 100 µM produced an average of .-0.00521±0.002; (d) 125 µM produced an average of 0.00648±.006 with all units in µU/200ng protein.

Recall the fact that acrolein is stabilized with hydroquinone due to its innate chemical properties at standard temperature and pressure. As a result, in order to contribute PARP activation to acrolein instead of hydroquinone, simultaneous exposure of cardiomyocytes to hydroquinone was performed. As shown in Figure 7, the amount of PARP activity detected from 125 μM and 50 μM acrolein-exposed cells was considerably higher (22 times and 8.69 times, respectively) than the amount detected from cells exposed to 125 μM and 50 μM of hydroquinone. In addition, the amount of PARP activity detected from 100 μM and 75 μM acrolein-exposed cells was about the same (1.627 times and 1.052 times, respectively) as that detected from corresponding hydroquinone-exposed cells.

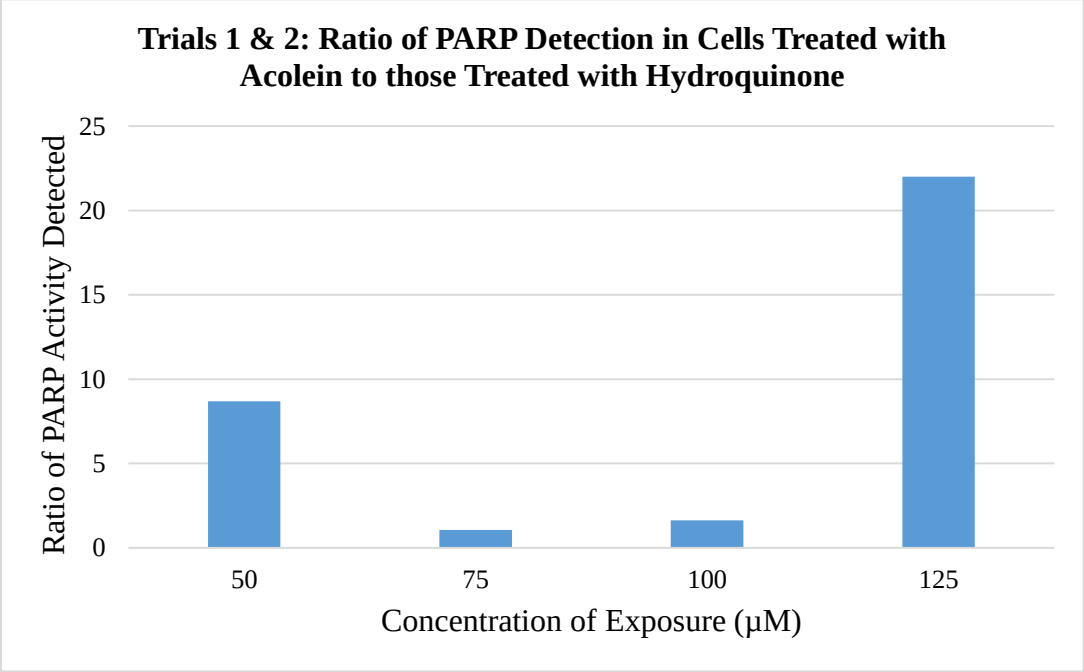

Figure 7: Trial 1 & 2: Ratio of PARP detection in cells treated with acrolein to those treated with hydroquinone. Depiction of the ratio of acrolein exposure with respect to hydroquinone exposure for corresponding concentrations. Hydroquinone exposures were adjusted to account for the percent of hydroquinone used to stabilize the acrolein (0.3%).

PARP Activity Detection Results from Trial 3

PARP activity detection upon cardiomyocyte exposure to varying acrolein concentrations had less numerical variation in trial three, with the highest return resulting from an acrolein concentration of 75 µM. As illustrated in Figure 8, PARP activity was measured over an exposure duration of fifty-five minutes (all with the units of micro units of PARP activity for 400ng of protein per well) and an acrolein concentration of 50µM produced an average PARP activity detection of 0.00260±0.002; exposure to an acrolein concentration of 75 µM produced an average of 0.00402±0.001; an acrolein concentration of 100 µM produced an average PARP activity detection of 0.00286±0.001; exposure to an acrolein concentration of 125 µM produced an average PARP activity detection of 0.00226±0.001.

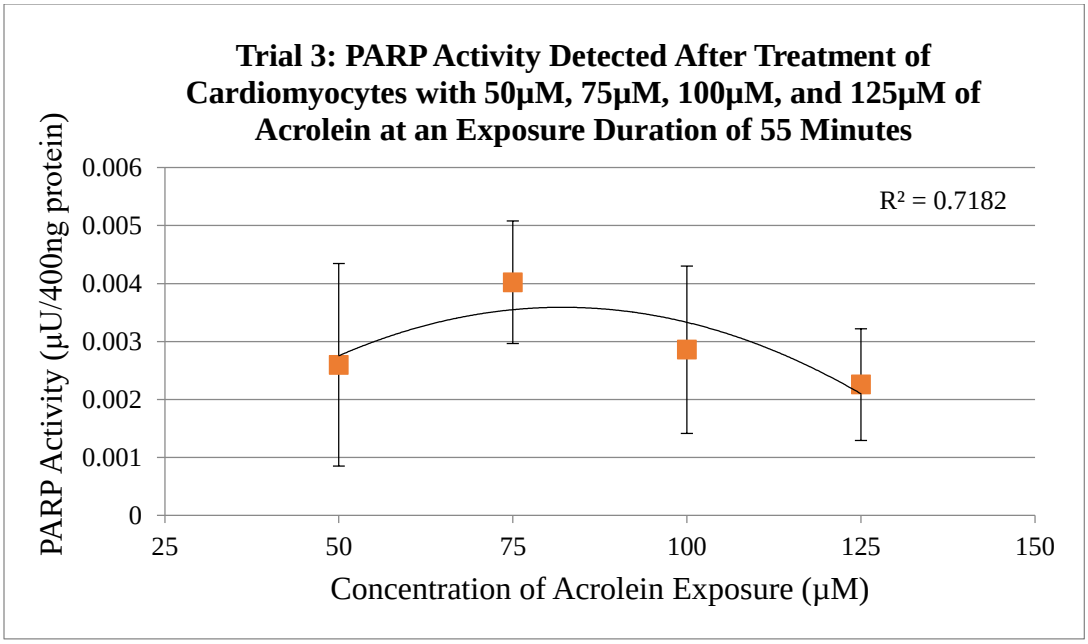

Figure 8: Trial 3: PARP activity detected after treatment of cardiomyocytes with 50 µM, 75 µM, 100 µM, and 125 µM of acrolein at an exposure duration of 55 minutes. Acrolein concentrations of (a) 50 µM produced an average of 0.00260±0.002; (b) 75 µM produced an average of 0.00402±0.001; (c) 100 µM produced an average of 0.00286±0.001; (d) 125 µM produced an average of 0.00226±0.001, with all units of µU/400ng protein. All averages were blanked against the lysis buffer control in order to account for possible interference.

All PARP activity averages were blanked against the lysis buffer control on its corresponding plate in order to account for possible interference. The standard curve for this PARP assay for plate one produced an R^2 value of 0.999 and the standard curve for this PARP assay for plate two had an R^2 value of 0.989. For Figure 8, the R^2 value for the polynomial line of best fit was 0.718.

Similarly to trials 1 and 2, cells treated with varying concentrations of hydroquinone were also evaluated for PARP activation. As shown in Figure 9, the amount of PARP detected from hydroquinone-exposed cells was about the same as that detected from acrolein-exposed cells, as all ratios were around 1.0. The concentration of 100µM produced a somewhat higher ratio, reflective of data obtained from the ratio of PARP detection in acrolein versus hydroquinone-treated cells from trials one and two.

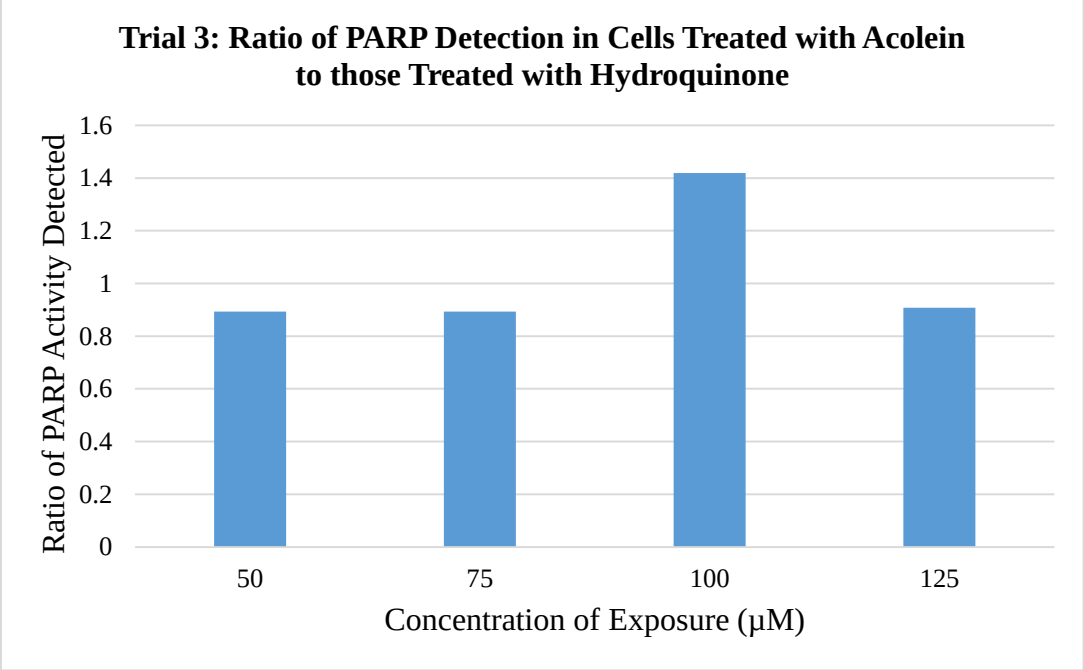

Figure 9: Trial 3: Ratio of PARP detection in cells treated with acrolein to those treated with hydroquinone. Depiction of the ratio of acrolein exposure with respect to hydroquinone exposure for corresponding concentrations. Hydroquinone exposures were adjusted to account for the percent of hydroquinone used to stabilize the acrolein (0.3%).

All PARP Activity Detection Results

In order to more effectively navigate the resulting PARP activities, data from all trials was combined. However, due to small sample size and different units, it is ignorant to assume variances of all trials are equal. To account for this, the larger of the two standard deviations were evaluated against the averaged standard deviations. For exposures of 75 and 100µM, these deviations remained the same. The PARP assay for trials one and two was performed at the same time under the same conditions. The PARP assay for trial three was performed at a later date under different human factor conditions but under the same laboratory conditions. As illustrated in Figure 10, PARP activity detection was assessed for varying concentrations of acrolein (all with the units, µU/200-400ng protein). An acrolein concentration of 50 µM produced an average PARP activity detection of 0.00150±0.001; exposure to an acrolein concentration of 75 µM produced an average PARP activity detection of 0.00569±0.001; an acrolein concentration of 100 µM produced an average PARP activity detection of -0.00118±0.002; exposure to an acrolein concentration of 125 µM produced an average PARP activity detection of 0.00145±0.004.

In Figure 10, the line of best fit assumed a polynomial of order three (R^2=1), predicting the highest averaged protein concentration to be around 67µM (blue) for all trials. However, because this data is simple with a linear prediction, a trendline characteristic of a polynomial of order two was also examined, producing an R^2 value of 0.0921. As this is an average from previous experiments, all averages were blanked against the lysis buffer control according to the aforementioned and the standard curves resulted in R^2 values ranging from 0.985 to 0.999, as mentioned above.

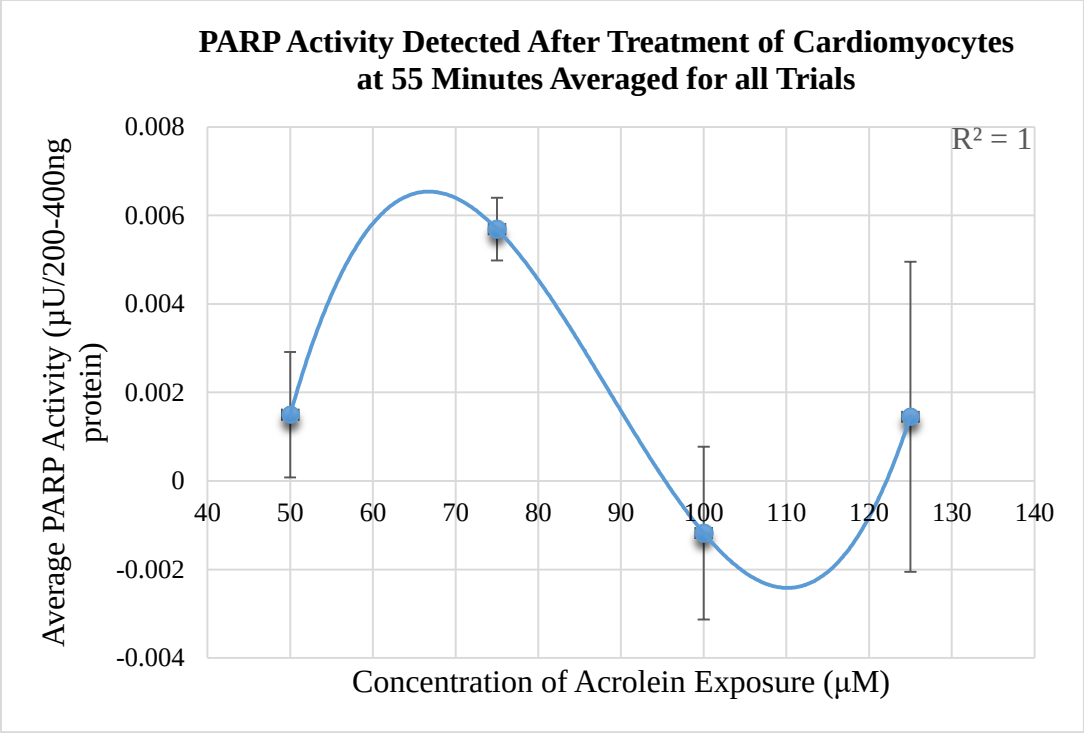

Figure 10: Average PARP activity detected after treatment of cardiomyocytes at 55 mins averaged for all trials. All had units of µU/200-400ng protein. Acrolein concentrations of (a) 50 µM produced an average of 0.00150±0.001; (b) 75 µM produced an average of 0.00569±0.001; (c) 100 µM produced an average of -0.00118±0.002; (d) 125 µM produced an average of 0.00145±0.004.

Summary of Results

PARP was activated at exposure concentrations of 75 µM in all trials, with an average detection of 0.00569 ± 0.001 µU/200-400ng protein. As shown in Figures 6, 8, and 10, standard deviation is relatively small, demonstrating lower variance and thus assigning more significance to the result. PARP may or may not have been activated at exposure concentrations of 50 µM, with average detection of 0.000402 ± 0.001 µU/200ng protein in trials 1 & 2, and an average detection of 0.00260 ± 0.002 µU/400ng protein; in trial 3. PARP may or may not have been activated at exposure concentrations of 100 µM due to low values (detection of 0.00286 ± 0.001 µU/200ng protein in the first two trials; -0.00118 ± 0.002 µU/400ng protein; in trial 3). PARP may or may not have been activated at exposure concentrations of 125 µM, as standard

deviations were comparatively very large in the first two trials. Ignoring large standard deviations, PARP was activated at acrolein exposure concentrations of 125 µM. Overall, the ratios determined from comparing the PARP activities detected from acrolein-exposed cells (stabilized with 0.3% hydroquinone) and the PARP activities detected from 0.3% hydroquinone-exposed cells demonstrate that the hydroquinone could have been masking the effects of PARP activation, could have been solely responsible for PARP activation, or other outstanding factors could have contributed. However, the considerably higher ratios of PARP activation from acrolein-exposed cells (concentrations of 50 µM and 100 µM) compared to PARP activation from hydroquinone-exposed cells (concentrations of 50 µM and 100 µM) in trials 1 & 2 suggest that the PARP activities detected was attributable to acrolein.

CHAPTER FOUR

Discussion

Throughout this process, treatment specifics were modified in order to increase accuracy and efficacy of experimental trials. In the initial trial, exposure duration was optimized by holding acrolein concentrations constant. The acrolein concentration of 75µM was chosen due to its relevance and inclusion in standard *in vitro* exposure practices (Wang et al., 2011; Luo et al. 2007). The exposure duration of 55 minutes was chosen due to its consistency with the aforementioned literature. The standard deviation for 25 minutes and 75 minutes was much lower than that observed for an exposure duration of 55 minutes. This could be due to individualized sampling that occurred for each plate: the plates with the lowest time and highest time were not subject to the same time constraints imposed on protein isolate and lysate extraction. For future testing and further optimization of acrolein and hydroquinone exposure durations, multiple plates could be tested at varying exposure durations in many subsets. In other words, the testing of exposure durations of 25 minutes, 55 minutes, and 75 minutes could have been divided into three consecutive but distinct sections, each with multiple plates staggered with different start times. This would act to tighten up the data by decreasing standard deviations.

For the initial trial, the PARP assay was run assuming 200 nanograms (ng) of protein per well would be sufficient for capturing PARP activity. This number was determined based on the unknown PARP nuclear fraction and studies conducted on a HepG2 cells in response to H_2O_2 exposures. Calculating appropriate solvent volumes and subsequent sample dilutions was based

on this assumption. Because detection of PARP-1 activity measured using the PARP assay in this trial was minimal, the 200 ng of protein per well assumption was increased to 400 ng of protein per well for all subsequent trials. This permitted appropriate dilutions with an increased probability of capturing intact PARP-1 activity. Reflected in the data, this modification achieved its goal.

As the trials were performed, refinement with respect to the lysis buffer control was also made. In the original trial, the lysis buffer control absorbance was read on an unrelated sample, as all of the lysis buffer was consumed in the process of cell treatment. This detergent is extremely important in that it destroys the membranes and permits a pH-controlled lysate to be obtained. Potential differences in concentrations could have resulted in minute differences between absorbances. As the unknown samples from each trial were blanked against the lysis buffer control, these small differences could drastically impact the results.

The results from trials one and two showed that the amount of PARP activity detected from 125μM and 50μM acrolein-exposed cells was considerably higher (22 times and 8.69 times, respectively) than the amount detected from cells exposed to 125μM and 50μM of hydroquinone, with 125μM producing a detection that was 253.2% that of the 50μM exposure. This implies acrolein activates PARP. In addition, the amount of PARP activity detected from 100 μM and 75 μM acrolein-exposed cells was about the same as that detected from corresponding hydroquinone cells (with 100 μM having a 108.3% detection with respect to 75 μM). This implies acrolein may or may not activate PARP. Data from trials one, two, and three produced results with high standard deviations but relatively low variance.

Interestingly enough, the amount of PARP activity obtained from cells treated with acrolein was about the same as that of cells treated with hydroquinone. This could be explained

by a failure to maintain a strict pH throughout all wells and throughout all procedural steps. However, the ratio of PARP detection in cells treated with acrolein to those treated with hydroquinone became more distinct in trial three. The differences between PARP activity for acrolein and hydroquinone as time went on might be indicative of learning through repetition and reflect increased accuracy with increased trial number.

As with all major experimental studies, data discrepancies resulting in high standard deviations could be impacted by human error. As is reflected by the data, standard deviations (and therefore variances) became smaller with more advanced trials. This is indicative of laboratory technique enhancement. Advancement of lab techniques could also account for potential environmental conditions: potential differences between plates could have existed in the time elapsed between complete individual exposures of each well and placement in controlled conditions (i.e., the incubator with a humidified atmosphere of 5% CO_2 at 37°C). In addition to these potential environmental differences, deviation from standard trypsinization procedures for H9c2 (2-1) occurred as the cells were centrifuged at room temperature instead of 4°C due to equipment restrictions (ATCC, 2014; Moreira et al., 2014; Louch et al., 2011; Engel et al., 1999). However, it is important to note that all of the cell viabilities fell within the expected range as pre-determined by American Type Culture Collect, and therefore no revisions were made to propagation or trypsinization procedures between trials.

In order to increase the number and accuracy of data points and to further elucidate the role of PARP-1 inhibition in reducing acrolein toxicity, methodology and techniques should be refined. Increasing the number of samples engenders statistical power and associated increased significance (Noordzij et al., 2009). As a result, increasing the number of samples run for different durations should be performed in a future experiment. Based on the results from this

study, additional increases in protein density should be examined as a method for increasing the chances of capturing PARP activity. Different exposure durations should also be evaluated within smaller increments, such as every five minutes. Decreasing the intervals could potentially result in a more increased protein return and a more accurate calculation of intact PARP-1 activity. In addition, different concentrations of acrolein and hydroquinone could be assessed to determine more pronounced toxicities. Adding a few extra concentrations that exceed 125µM could be beneficial for a more thorough investigation into the acute toxic endpoints associated with the exposure of H9c2(2-1) to acrolein.

Further testing involving the use of Western blotting techniques should be performed for qualitative data which will identify the specific amino-acid sequences after protein isolation and quantification. This has the potential to detect specific translocations and caspase cleavages which will definitively link the occurring processes to observed data. Further elucidation of caspase involvement can be uncovered with the inclusion of fluorescent microscopy. This technique involves flurochrome staining of nucleic components. Depending on the fluorescent lifetime, these components communicate back through the emission of different wavelengths. This technique permits individualized selection for execution or initiator caspases and can identify and label active caspases within cells (Reviewed in Grabarek et al., 2002). This technique can delineate between types of cell death and quantify apoptosis which would be beneficial for further investigation into the role between PARP and acrolein-induced toxicities (Ribble et al., 2005).

In addition to the aforementioned, other common drug interferences should be investigated. One of the most important confounders is sodium-2-mercaptoethane sulfonate, $C_2H_5NaO_3S_2$, which is often given to patients to alleviate dose-limiting symptoms. As the name

suggests, this thiol compound is a sulfhydroyl donor. Upon intravenous delivery to a patient, this drug readily oxidizes in systemic circulation to disodium-2,2'-dithio-bis-ethane sulfonate, which is pharmacologically inert (Masuda et al., 2011). It is further reduced to mesna (trade name: Mesnex^{TM}) in the kidneys and then the free sulfhydroyl group acts through conjugate addition to bind to and inactivate the very electrophilic (i.e., sulfhydroyl acceptor) acrolein in the bladder before acrolein has time to interact with cardiac muscle tissue (Kurowski & Wagner, 1997). The nontoxic conjugates are excreted in urine (Brock et al., 1982). This chemo-protectant drug is commonly prescribed to patients undergoing therapeutic regimens that include the use of nitrogen mustards, due to its ability to prevent drug-induced hemorrhagic cystitis and hematuria without altering the chemotherapeutic effects of antineoplastics (Altayli et al., 2012; Manikandan et al., 2010; Andriole et al., 1987). Although the effects of mesna on drug-induced cardiotoxicity has yet to be experimentally elucidated, its mechanism of action implies mesna's relevance in reducing acrolein-induced cytotoxicity. Therefore, further tests with the inclusion of mesna should be performed.

CHAPTER FIVE

Conclusion

Due to the clinical implications from acrolein-induced cardiotoxicity, and ethical considerations with *in vivo* models, formation of an *in vitro* method of analysis is paramount. This research sought to determine whether or not the H9c2 (2-1) cardiomyocyte cell line was an appropriate model for evaluating the change in poly (ADP-ribose) polymerase (PARP) activity with acrolein-induced cellular toxicity. Multiple studies have gauged the efficacy of this cell line through numerous types of research, which is accentuated through the viability assessment performed in this study and the continued propagation success of the line. An exposure duration of fifty-five minutes was chosen due to its high detection and variation in protein concentrations obtained from acrolein-treated cells with respect to the control. Protein concentrations, determined via the BCA Protein Quantification Assay, were high enough for most wells to undergo appropriate dilutions for the PARP assay. The PARP assay permitted evaluation of PARP-1 activity. In most circumstances, hydroquinone-exposed cells had roughly the same subsequent PARP-1 activity as acrolein-exposed cells. This implies that the hydroquinone could have been concealing the effects of acrolein exposure. PARP-1 was activated at exposure concentrations of 75 μM in all trials. Other concentrations showed potential PARP activity. Thus, this model can be refined and used for further characterization of the role of PARP in acrolein-induced cardiomyopathy.

REFERENCES

Ahel, I., Ahel, D., Matsusaka, T., Clark, A. J., Pines, J., Boulton, S. J., and West, S. C. (2008). Poly(ADP-ribose)-binding zinc finger motifs in DNA repair/checkpoint proteins. Nature, *451*(7174), 81-85.

Altayli, E., Malkoc, E., Alp, B. F. & Korkmaz, A. (2012) Prevention and treatment of cyclophosphamide and ifosfamide-induced hemorrhagic cystitis. *Journal of Molecular Pathophysiology, 1*(1), 53-62. doi:10.5455/jmp.20120321060902

Altmeyer, M., Messner, S., Hassa, P. O., Fey, M., and Hottiger, M. O. (2009). Molecular mechanism of poly(ADP-ribosyl)ation by PARP1 and identification of lysine residues a ADP-ribose acceptor sites. *Nucleic Acids Research, 37*(11), 3723–3738. doi:10.1093/nar/gkp229

Amé, J.C., Spenlehauer, C., and deMurcia, G. (2004). The PARP superfamily. *BioEssays, 26*, 882–893. doi: 10.1002/bies.20085

Anderson, D., Bishop, J. B., Garner, R. C., Ostrosky-Wegman, P., and Selby, P. B. (1995). Cyclophosphamide: Review of its mutagenicity for an assessment of potential germ cell risks. *Mutation Research/Fundamental and Molecular Mechanisms of Mutagenesis, 330*(1-2), 115-181.

Andrabi, S.A., Kim, N.S., Yu, S.W., Wang, H., Koh, D.W., Sasaki, M. et al. (2006). Poly(ADP ribose) (PAR) polymer is a death signal. *Proceedings of the National Academy of Sciences, 103*(48), 18308-18313.

Andriole, G.L., Sandlund, J.T., Miser, J.S., Arasi, V., Linehan, M., and Magrath, I.T. (1987). The efficacy of mesna (2-mercaptoethane sodium sulfonate) as a uroprotectant in patients with hemorrhagic cystitis receiving further oxazaphosphorine chemotherapy. *Journal of Clinical Oncology, 5*(5), 799-803.

Appelbaum, F.R., Strauchen, J.A., Graw, R.G., Savage, D.D., Kent, K.M., Ferrans, V.J., and Herzig, G.P. (1976). Acute lethal carditis caused by high-dose combination chemotherapy. A unique clinical and pathological entity. *Lancet, 1,* 58-62.

Arntz, D., Fischer, M., Höpp, M., Jacobi, S., Sauer, T., Ohara, T., Sato, N., Shimizu, N., and Schwind, H. (2012). Acrolein and Methacrolein. *Ullmann's Encyclopedia of Industrial Chemistry*. Weinheim, Germany: Wiley-VCH.

ATCC. (2014). Product sheet for H9c2(2-1) (ATCC® CRL-1446™). Retrieved from www.atcc.org/~/ps/CRL-1446.ashx

ATSDR. (2007). Toxicological profile for acrolein. *US Department of Health and Human Services – Agency for Toxic Substances and Disease Registry*, 1-207.

Banasik, M., Stedeford, T., et al. (2004). The effects of organic solvents on poly (ADP-ribose) polymerase-1 activity: implications for neurotoxicity. *Acta Neurobiologiae Experimmentalis, 64*(4), 467-473. Accessed from pubmed.gov on 21 November 2015.

Beck, C., Robert, I., Reina-San-Martin, B., Schreiber, V., and Dantzer, F. (2014). Poly(ADP ribose) polymerases in double-strand break repair: focus on PARP1, PARP2 and PARP3. *Experimental Cell Research, 329*(1), 18-25.

Bergh, J., Wiklund, T., Erikstein, B., et al. (1998). Dosage of adjuvant G-CSF (filgrastim)-supported FEC polychemotherapy based on equivalent haematological toxicity in high-risk breast cancer patients. Scandinavian Breast Group, Study SBG 9401. *Annals of Oncology, 9*(4), 403–411.

Bignold, L. P. (2006). Alkylating agents and DNA polymerases. *Anticancer Research, 26*, 1327-1336.

Bontenbal, M., Andersson, M., Wildiers, J., et al. (1998). Doxorubicin vs epirubicin, report of a second-line randomized phase II/III study in advanced breast cancer. EORTC Breast Cancer Cooperative Group. *British Journal of Cancer, 77*(12), 2257-2263.

Branco, A.F., Pereira, S.P., Gonzalez, S., Gusev, O., Rizvanov, A.A., and Oliveira, P.J. (2015). Gene expression profiling of H9c2 myoblast differentiation towards a cardiac-like phenotype. *PLoS ONE, 10*(6), e0129303. doi: 10.1371/journal.pone.0129303.

Braverman, A.C., Antin, J.H., Plappert, M.T., Cook, E.F., and Lee, R.T. (1991). Cyclophosphamide cardiotoxicity in bone marrow transplantation: a prospective evaluation of new dosing regimens. *Journal of Clinical Oncology, 9*, 1215-1223.

Brock, N., Pohl, J., Stekar, J., and Scheef, W. (1982). Studies on the urotoxicity of oxazaphosphorine cytostatics and its prevention—III: Profile of action of sodium 2 mercaptoethane sulfonate (mesna). *European Journal of Cancer and Clinical Oncology, 18*, 1377-1387.

Brockstein, B.E., Smiley, C., Al-Sadir, J., Williams, S.F. (2000). Cardiac and pulmonary toxicity in patients undergoing high-dose chemotherapy for lymphoma and breast cancer: prognostic factors. *Bone Marrow Transplant, 25*, 885-894.

Bunting, K. D., and Townsend, A. J. (1998). Dependence of aldehyde dehydrogenase-mediated oxazaphosphorine resistance on soluble thiols: importance of thiol interactions with the secondary metabolite acrolein. *Biochemical Pharmacology, 56*(1), 31-39.

Chen, C. S., Lin, J. T., Goss, K. A., et al. (2004). Activation of the anticancer prodrugs cyclophosphamide and ifosfamide: Identification of cytochrome P450 2B enzymes and site-specific mutants with improved enzyme kinetics. *Molecular Pharmacology, 65*(5), 1278-1285.

Chen, J., Guo, R., Yan, H., Tian, L., You, Q., Li, S., Huang, R. and Wu, K. (2014). Naringin inhibits ROS-activated MAPK pathway in high glucose-induced injuries in H9c2 cardiac cells. *Basic & Clinical Pharmacology & Toxicology, 114*, 293–304.

Chen, M., Zsengeller, Z., Xiao, C.Y., and Szabó, C. (2004). Mitochondrial-to-nuclear translocation of apoptosis-inducing factor in cardiac myocytes during oxidant stress: potential role of poly(ADP-ribose) polymerase-1. *Cardiovascular Research, 63,* 682-688.

Chlebowski, R. T. (1979). Adriamycin (doxorubicin) cardiotoxicity: A review. *Western Journal of Medicine, 131*(5), 364-368.

Colvin, M. (2003). Alkylating Agents. In: Kufe DW, Pollock RE, Weichselbaum RR, et al., editors. Holland-Frei Cancer Medicine. 6th edition. Hamilton (ON): BC Decker. Available from: http://www.ncbi.nlm.nih.gov/books/NBK12772/.

Conklin, D.J., Haberzettl, P., et al. (2015). Glutathione S-transferase P protects against ‘ cyclophosphamide-induced cardiotoxicity in mice. *Toxicology and Applied Pharmacology, 285*(2), 136-148.

D'Amours, D., Desnoyers, S., D'Silva, I., and Poirier, G. G. (1999). Poly(ADP-ribosyl)ation reactions in the regulation of nuclear functions. *Biochemical Journal, 342*(Pt 2), 249-268.

Daugherty, M.D., Young, J.M., Kerns, J.A., and Malik, H.S. (2014). Rapid evolution of PARP genes suggests a broad role for ADP-Ribosylation in host-virus conflicts. *PLoS Genetics, 10*(5), e1004403. doi: 10.1371/journal.pgen.1004403

De Vos, M., Schreiber, V., and Dantzer, F. (2012). The diverse roles and clinical relevance of PARPs in DNA damage repair: current state of the art. *Biochemical Pharmacology, 84*, 137-146.

Dong, L., Zhou, S., et al. (2013). Magnolol protects against oxidative stress-mediated neural cell damage by modulating mitochondrial dysfunction and PI3K/Akt signaling. *Journal of Molecular Neuroscience, 50,* 469-481.

Dow, E., Schulman, H. & Agura, E. (1993). Cyclophosphamide cardiac injury mimicking acute myocardial infarction. *Bone Marrow Transplant, 12,* 169-172.

Drew, Y. (2015). The development of PARP inhibitors in ovarian cancer: from bench to bedside. *British Journal of Cancer, 113*, S3-S9. doi: 10.1038/bjc.2015.394

Eliasson, M. J., Sampei, K., Mandir, A. S., et al. (1997). Poly (ADP-ribose) polymerase gene disruption renders mice resistant to cerebral ischemia. *Nature medicine, 3*(10), 1089-1095.

Engel, F.B., Hauck, L., Cardoso, M.C., Leonhardt, H., Dietz, R., and VonHarsdorf, R. (1999). A mammalian myocardial cell-free system to study cell cycle reentry in terminally differentiated cardiomyocytes. Circulation Research, *85*, 294-301.

EPA. (2015). Method 603: Acrolein and acrylonitrile. *United States Environmental Protection Agency*, 1-21. (Originally published in 1984).

Erener, S., Hesse, M., Kostadinova, R., and Hottiger, M. (2011). Poly(ADP-Ribose)Polyermase 1 (PARP1) controls adipogenic gene expression and adipocyte function. *Molecular Endocrinology*, 26(1). doi: 10.1210/me.2011-1163#sthash.F35vqoRB.dpuf

Erselcan, T., Kairemo, K. J. A., Wiklund, T. A., et al. (2000). Subclinical cardiotoxicity following adjuvant dose-escalated FEC, high-dose chemotherapy, or CMF in breast cancer. *British Journal of Cancer*, *82*(4), 777–781. doi: 10.1054/bjoc.1999.0998

Eustermann, S., Videler, H., Yang, J. C., Cole, P. T., Gruszka, D., Veprintsev, D., and Neuhaus, D. (2011). The DNA-binding domain of human PARP-1 interacts with DNA single strand breaks as a monomer through its second zinc finger. *Journal of molecular biology*, *407*(1), 149-170.

Fatokun, A. A., Dawson, V. L., and Dawson, T. M. (2014). Parthanatos: mitochondrial-linked mechanisms and therapeutic opportunities. *British Journal of Pharmacology, 171*(8), 2000–2016.

Federman, D. G., and Henry, G. (1997). Chemotherapy-induced myocardial necrosis in a patient with chronic lymphocytic leukemia. *Respiratory Medicine, 91*(9), 565-567.

Feenstra, J., Grobbee, D. E., et al. (1999). Drug-induced heart failure. *Journal of Molecular and Cellular Cardiology, 33*(5), 1152-1162. doi: 10.1016/S0735-1097(99)00006-6

Fiorillo, C., Pace, S., Ponziani, V., Nediani, C., Perna, A. M., et al. (2002). Poly(ADP-ribose) polymerase activation and cell injury in the course of rat heart heterotopic transplantation. *Free Radical Research, 36*, 79-87.

Fiorillo, C., Ponziani, V., Giannini, L., Cecchi, C., Celli, A., et al. (2003). Beneficial effects of poly(ADP-ribose) polymerase inhibition against the reperfusion injury in heart transplantation. *Free Radical Research, 37*, 331-339.

Fitzakerley, J. L. (2015). Antineoplastics: Cell cycle specificity [Lecture notes]. Retrieved from http://www.d.umn.edu/~jfitzake/Lectures/DMED/Antineoplastics/GeneralConcepts/CellCycleSpecificity.html.

Foo, J., and Michor, F. (2014). Evolution of acquired resistance to anti-cancer therapy. *Journal of Theoretical Biology, 0,* 10-20. doi 10.1016/j.jtbi.2014.02.025

Frank-Vaillant M., and Marcand, S. (2002). Transient stability of DNA ends allows nonhomologous end joining to precede homologous recombination. *Molecular Cell, 10*(5), 1189- 1199.

Frei, E III., and Eder, JP. (2003). Combination Chemotherapy. In: Kufe DW, Pollock RE, Weichselbaum RR, et al., editors. Holland-Frei Cancer Medicine. 6th edition. Hamilton (ON): BC Decker; 2003.

Gerö, D., Szoleczky, P., Chatzianastasiou, A., Papapetropoulos, A., and Szabó, C. (2014). Modulation of Poly(ADP-ribose) polymerase-1 (PARP-1)-mediated oxidative cell injury by ring finger protein 146 (RNF146) in cardiac myocytes. *Molecular Medicine, 20*(1), 313–328. doi: 10.2119/molmed.2014.00102

Gluck, S. (2005). Adjuvant chemotherapy for early breast cancer: Optimal use of epirubicin. *The Oncologist, 10*(10), 780-791.

Goldberg, M.A., Antin, J.H., Guinan, E.C., & Rappeport, J.M. (1986). Cyclophosphamide cardiotoxicity: an analysis of dosing as a risk factor. *Blood, 68*(5), 1114-1118.

Gottdiener, J.S., Appelbaum, F.R., Ferrans, V.J., Deisseroth, A., and Ziegler, J. (1981). Cardiotoxicity associated with high-dose cyclophosphamide therapy. *JAMA, 141,* 758-763.

Grabarek, J., Amstad, P., and Darzynkiewicz, Z. (2002). Use of fluorescently labeled caspase inhibitors as affinity labels to detect activated caspases. *Human Cell, 15,* 1–12.

Griskevicius, L., Yasar, U., Sandberg, M., et al. (2003). Bioactivation of cyclophosphamide: the role of polymorphic CYP2C enzymes. *European Journal of Clinical Pharmacology, 59*(2), 103-109.

Hales, B. F. (1982). Comparison of the mutagenicity and teratogenicity of cyclophosphamide and its active metabolites, 4-Hydroxycyclophosphamide, phosphoramide mustard, and acrolein. *Cancer Research, 42,* 3016-3021.

Hall, I. H. (1980). The anticancer drugs. Article by Pratt, W. B., and Ruddon, R. W. (1979). *Journal of Pharmaceutical Sciences, 69,* 484. doi: 10.1002/jps.2600690439

Hardman, J. G., Limbird, L. E., Molinoff, P.B., et al. (1996). *Goodman and Gilman's The Pharmacological Basis of Therapeutics.* 9th edition. NY, NY: McGraw-Hill, p. 1395.

Hassa, P. O., and Hottiger, M. O. (2008). The diverse biological roles of mammalian PARPs, a small but powerful family of poly-ADP-ribose polymerases. *Frontiers in bioscience, 13,* 3046-3082.

Helsby, N. A., Hui, C. Y., Goldthorpe, M. A., et al. (2010). The combined impact of CYP2C19 and CYP2B6 pharmacogenetics on cyclophosphamide bioactivation. *British Journal of Clinical Pharmacology, 70*(6), 844-853.

Hescheler, J., Meyer, R., Plant, S., Krautwurst, D., Rosenthal, W., and Schultz, G. (1991). Morphological, biochemical, and electrophysiological characterization of a clonal cell (H9c2) line from rat heart. *Circulation Research, 69,* 1476-1486.

Horton, N. D., Biswal, S. S., Corrigan, L. L., Bratta, J., and Kehrer, J. P. (1999). Acrolein causes inhibitor kappaB-independent decreases in nuclear factor kappaB activation in human lung adenocarcinoma (A549) cells. *Journal of Biological Chemistry, 274,* 9200–9206.

Housman, G., Byler, S., Heerboth, S., et al. (2014). Drug resistance in cancer: An overview. *Cancers, 6*(3), 1769-1792. doi:10.3390/cancers6031769

Huang, Z., Roy, P., and Waxman, D. J. (2000) Role of human liver microsomal CYP3A4 and CYP2B6 in catalyzing N-dechloroethylation of cyclophosphamide and ifosfamide. *Biochemical Pharmacology, 59,* 961-972.

Ikejima, M., Noguchi, S., Yamashita, R., Ogura, T., Sugimura, T., Gill, D. M., and Miwa, M. (1990). The zinc fingers of human poly(ADP-ribose) polymerase are differentially required for the recognition of DNA breaks and nicks and the consequent enzyme activation. Other structures recognize intact DNA. *Journal of biological chemistry, 265*(35), 21907-21913.

Inoue, T., Tanaka, K., Mishima, M., and Watanabe, K. (2008). Predictive *in vitro* cardiotoxicity and hepatotoxicity screening system using neonatal rat heart cells and rat hepatocytes. *Japanese Society for Alternatives to Animal Experiments, 14,* Special Issue, 457-462.

Ismahil M. A., Hamid, T., Haberzettl, P., Gu, Y., Chandrasekar, B., Srivastava, S., Bhatnagar, A., and Prabhu, S. D. (2011). Chronic oral exposure to the aldehyde pollutant acrolein induced dilated cardiomyopathy. *American Journal of Physiology – Heart and Circulatory Physiology, 301*(5), H2050-2060. doi: 10.1152/ajpheart.00120.2011

Jagtap, P., and Szabó, C. (2005). Poly(ADP-ribose) polymerase and the therapeutic effects of its inhibitors. *Nature Reviews Drug Discovery, 4*(5), 421-440.

Jamieson, D., Lee, J., Cresti, N., Jackson, R., et al. (2014). Pharmacogenetics of adjuvant breast cancer treatment with cyclophosphamide, epirubicin and 5-fluorouracil. *Cancer Chemotherapy Pharmacology, 74,* 667-674.

Juma, F.D., Rogers, H.J., and Trounce, J.R. (1979). Pharmacokinetics of cyclophosphamide and alkylating activity in man after intravenous and oral administration. *British Journal of Clinical Pharmacology, 8,* 209-217.

Kameoka, M., Ota, K., Tetsuka, T., Tanaka, Y., Itaya, A., Okamoto, T., and Yoshihara, K. (1999). Evidence for regulation of NF-kappaB by poly(ADP-ribose) polyermase. *Biochemical Journal, 346*(Pt3), 641-649.

Kameshita, I., Matsuda, Z., Taniguchi, T., and Shizuta, Y. (1984). Poly (ADP-Ribose) synthetase. Separation and identification of three proteolytic fragments as the substrate binding domain, the DNA-binding domain, and the automodification domain. *Journal of biological chemistry, 259*(8), 4770-4776.

Kamezaki, K., Fukuda, T., Makino, S. & Harada, M. (2005). Cyclophosphamide-induced cardiomyopathy in a patient with seminoma and a history of mediastinal irradiation. *Internal Medicine, 44*(2), 120-123.

Katayama M, Imai Y, Hashimoto H, Kurata M, Nagai K, Tamita K, Morioka S, and Furukawa Y. (2009). Fulminant fatal cardiotoxicity following cyclophosphamide therapy. *Journal of Cardiology*, 54, 330-334.

Kehrer, J. P., and Biswal, S.S. (2000). The molecular effects of acrolein. *Toxicological Sciences, 57*, 6-15.

Kimes, B.W., and Brandt, B.L. (1976). Properties of a clonal muscle cell line from rat heart. *Experimental Cell Research, 98,* 367-381.

King, P. D., and Perry, M. C. (2001). Hepatotoxicity of chemotherapy. *The Oncologist, 6*(2), 162-176.

Kolthur-Seetharam, U., Dantzer, F., McBurney, M. W., de Murcia, G., and Sassone-Corsi, P. (2006). Control of AIF-mediated cell death by the functional interplay of SIRT1 and PARP-1 in response to DNA damage. *Cell Cycle, 5*(8), 873-877.

Kow, Y.W., and Doetsch, P.W. (2005). *DNA Damage Recognition.* W. Siede (Ed.) Boca Raton, FL: Taylor & Francis Group.

Kurowski, V., and Wager, T. (1997). Urinary excretion of ifosfamide, 4'-hydroxyifosfamide, 3- and 2-dechloroethylifosfamide, mesna and dimesna in patients on fractionated intravenous ifosfamide and concomitant mesna therapy. *Cancer Chemotherapy and Pharmacology, 39*(5), 431-439.

Li, X., Erden, O., Li, L., Ye, Q., Wilson, A., and Du, W. (2014). Binding to WGR Domain by Salidroside Activates PARP1 and Protects Hematopoietic Stem Cells from Oxidative Stress. *Antioxidants and Redox Signaling, 20*(12), 1853–1865. doi:10.1089/ars.2013.5600

Lin, Y., Tang, X., Zhu, Y., Shu, T., and Han, X. (2011). Identification of PARP-1 as one of the transcription factors binding to the repressor element in the promoter region of COX-2. *Archives of Biochemistry and Biophysics, 505*(1), 123-129.

Lonza Cologne GmbH. (2012). Protocol for performing a trypan blue viability test: Technical reference guide. *BioResearch*, 1-2. Accessed on 26 February 2016 from http://bio.lonza.com/uploads/tx_mwaxmarketingmaterial/Lonza_BenchGuides_Protocol_for_Performing_a_Trypan_Blue_Viability_Test__Technical_Reference_Guide.pdf.

LoPachin, R.M., Gavin, T., Petersen, D.R., and Barber, D.S. (2009). Molecular mechanisms of 4-hydroxy-2-nenenal and acrolein toxicity: Nucleophilic targets and adduct formation. *Chemical Research in Toxicology, 22*(9), 1499-1508. doi: 10.1021/tx900147g.

Louch, W. E., Sheehan, K. A., & Wolska, B. M. (2011). Methods in cardiomyocyte isolation, culture, and gene transfer. *J Mol Cell Cardiol, 51*(3), 288-298.

Luminari, S., and Federico, M. (2011). Case studies of elderly patients with non-Hodgkin's lymphoma. *Hematology Reports*, *3*(3 Suppl), e7. doi: 10.4081/hr.2011.s3.e7

Luo, J., Hill, B. G., Gu, Y., Cai, J., Srivastava, S., Bhatnagar, A., and Prabhu, S.D. (2007). Mechanisms of acrolein-induced myocardial dysfunction: implications for environmental and endogenous aldehyde exposure. *American Journal of Physiology, 293*(6). doi: 10.1152/ajpheart.00284.2007

Lupo, B., and Trusolino, L. (2014). Inhibtion of poly(ADP-ribosyl)ation in cancer: Old and new paradigms revisited. *Biochimica et Biophysica Acta*, *1846*(1), 201-215.

Makowski, G. S. (2015). *Advances in clinical chemistry*. Farmington, CT: Elsevier.

Manikandan, R., Kumar, S., and Dorairajan, L.N. (2010). Hemorrhagic cystitis: A challenge to the urologist. *Indian Journal of Urology, 26*(2) 159-166.

Masuda, N., Negoro, S., Hausheer, F., Nakagawa, K., Matsui, K., Kudoh, S., Takeda, K., Yamamoto, N., Yoshimura, N., Ohashi, Y., and Fukuoka, M. (2011). Phase I and pharmacologic study of BNP7787, a novel chemoprotector in patients with advanced non-small cell lung cancer. *Cancer Chemotherapy and Pharmacology, 67,* 533-542.

McCartan, C., Mason R., Jayasinghe, S. R., and Griffiths, L. R. (2012). Cardiomyopathy classification: Ongoing debate in the genomics era. *Biochemistry Research International,* vol. 2012, Article ID 796926. doi:10.1155/2012/796926

McCloskey, J. K., Broome, C. M., Cheson, B. D. (2013). Safe and effective treatment of aggressive Non-Hodgkin Lymphoma with Rituximab and Bendamustine in patients with severe liver impairment. *Clinical Advances in Hematology & Oncology, 11*(3), 184-189.

McDermott, M., Eustace, A. J., Busschots, S., Breen, L., Crown, J., Clynes, M., et al. (2014). *In vitro* development of chemotherapy and targeted therapy drug-resistant cancer cell lines: A practical guide with case studies. *Frontiers in Oncology, 4*, Article 40.

Menard, C., Pupier, S., Mornet, D., Kitzmann, M., Nargeot, J., and Lory, P. (1999). Modulation of L-type calcium channel expression during retinoic acid-induced differentiation of H9C2 cardiac cells. *Journal of Biological Chemistry, 274*(41), 29063–29070.

Micetich, K. C. (2014). Chemotherapy II: Alkylating agents [Lecture notes]. Retrieved from http://www.lumen.luc.edu/lumen/meded/therapy/homepage/PharmIIBlockIV_1314.pdf.

Moghe, A., Ghare, S., Lamoreau, B., Mohammad, M., Barve, S., McClain, C., and Joshi-Barve, S. (2015). Molecular mechanisms of acrolein toxicity: relevance to human disease. *Toxicological Sciences, 143*(2), 242-255. doi: 10.1093/toxsci/kfu233

Monaco, L., Kolthur-Seetharam, U., Loury, R., Murcia, J. M., DeMurcia, G., and Sassone-Corsi, P. (2005). Inhibition of Aurora-B kinase activity by poly(ADP-ribosyl)ation in response to DNA damage. *Proceedings of the National Academy of Sciences of the United States of America, 102*(40), 14244-14248.

Moore, M. J. (1991). Clinical pharmacokinetics of cyclophosphamide. *Clinical Pharmacokinetics, 20*(3), 194-208.

Moreira, A.C., Branco, A.F., Sampaio, S.F., Cunha-Oliveira, T., Martins, T.R., Holy, J., Oliveira, P.J., and Sardao, V.A. (2014). Mitochondrial apoptosis-inducing factor is involved in dosxorubicin-induced toxicity of H9c2 cardiomyoblasts. *Biochimica et Biophysica Acta – Molecular Basis of Disease, 1842*(12), 2468-2478.

Nagaraja, A. S., Sadaoui, N. C., Lutgendorf, S. K., et al. (2013). Beta blockers: A new role in chemotherapy. *Expert Opinion on Investigational Drugs, 22*(11), 1359-1363.

Nakamura, S., Aoki, M., Mori, A., Nakahara, T., Sakamoto, K., and Ishii, K. (2010). Analysis of cardiac toxicity caused by cyclophosphamide in the H9c2 cell line and isolated and perfused rat hearts. *Japanese Journal of Cancer and Chemotherapy, 37*(4), 677-680. PMID: 20414025

Newton, T. A. (1991). Inert atmosphere techniques for the microscale laboratory. *Journal of Chemical Education,* 68(3), A60.

Nicolai, S., Rossi, A., Di Daniele, N., Melino, G., et al. (2015). DNA repair and aging: the impact of the p53 family. *Aging*, 7(12), 1050-1065.

Nieto, Y., Cagnoni, P.J., Bearman, S.I., Shpall, E.J., Matthes, S., and Jones, R.B. (2000). Cardiac toxicity following high-dose cyclophosphamide, cisplatin, and BCNU (STAMP-I) for breast cancer. Biology of Blood and Marrow Transplantation, *6*, 198-203.

Nishikawa, T., Miyahara, E., Kurauchi, K., Watanabe, E., Okamoto, Y., and Kawano, Y. (2015). Mechanisms and prevention of fatal cardiotoxicity following high-dose cyclophosphamide therapy. *Blood*, *124*(21), 5789.

Nogueiras, R., Habegger, K. M., Chaudhary, N., Finan, B., Banks, A. S., Dietrich, M. O., Horvath, T.L., Sinclair D.A., Pfluger, P.T. and Tschöop, M. H. (2012). Sirtuin 1 and sirtuin 3: physiological modulators of metabolism. *Physiological Reviews*, *92*(3), 1479–1514.

Noordzij, M., Tripepi, G., Dekker, F.W., Zoccali, C., Tanck, M.W., and Jager, K.J. (2009). Sample size calculations: basic principles and common pitfalls. *Nephrology Dialysis Transplant, 25*, 1388-1393. doi: 10.1093/ndt/gfp732

Otto, H., Reche, P.A., Bazan, F., Dittmar, K., Haag, F., and Koch-Nolte F. (2005). In silico characterization of the family of PARP-like poly(ADP-ribosyl)transferases (pARTs). *BMC Genomics*, *6*, 139. doi:10.1186/1471-2164-6-139

Parry, H. L. (1948). Stabilization of acrolein. *U.S. Patent No. 2,653,172.* Washington, DC: U.S. Patent and Trademark Office.

Pasquier, E., Ciccolini, J., Carre, M., et al. (2011). Propranolol potentiates the anti-angiogenic effects and anti-tumor efficacy of chemotherapy agents: implication in breast cancer treatment. *Oncotarget*, *2*(10), 797-809. doi: 10.18632/oncotarget.343

Perina, D., Mikoč, A., Ahel, J., Ćetković, H., Žaja, R., and Ahel, I. (2014). Distribution of protein poly(ADP-ribosyl)ation systems across all domains of life. *DNA Repair, 23*, 4-16. doi: 10.1016/j.dnarep.2014.05.003

Petrilli, V., Herceg, Z., Hassa, P.O., Patel, N.S., DiPaola, R., Cortes, U., Dugo, L., Filipe, H.M., Thiemermann, C., Hottiger, M.O., Cuzzocrea, S., and Wang, Z.Q. (2004). Noncleavable poly(ADP-ribose) polymerase-1 regulates the inflammation response in mice. *The Journal of Clinical Investigation, 114*, 1072–1081.

Poirier, G., and Moreau, P. (1992). *ADP-Ribosylation Reactions.* (1st ed., pp. 92-95). New York, NY: Springer New York.

Preuss, C. (2015). Antineoplastics [PowerPoint slides]. Retrieved from usflearn.instructure.com.

Ren, S., Kalhorn, T. F., and Slattery, J. T. (1999). Inhibition of human aldehyde dehydrogenase 1 by the 4-hydroxycyclophosphamide degradation product acrolein. *Drug Metabolism and Disposition, 27*(1), 133-137.

Ribble, D., Goldstein, N. B., Norris, D. A., & Shellman, Y. G. (2005). A simple technique for quantifying apoptosis in 96-well plates. *BMC Biotechnology*, *5*, 12.

Roy, J., Pallepati, P., Bettaieb, A.et al. (2009). Acrolein induces a cellular stress response and triggers mitochondrial apoptosis in A549 cells. *Chemico-Biological Interactions, 181*(2): 154-167.

Roy, J., Pallepati, P., & Bettaieb, A. (2010). Acrolein induces apoptosis through the death receptor pathway in A549 lung cells: role of p53. *Canadian Journal of Physiology & Pharmacology, 88*(3), 353-368.

Ruf, A., deMurcia, G., and Schulz, G. E. (1998). Inhibitor and NAD+ binding to poly(ADPribose) polymerase as derived from crystal structures and homology modeling. *Biochemistry, 37*(11), 3893-3900.

Saberi, A., Hochegger, H., Szuts, D., Lan, L., Yasui, A., Sale, J. E., Taniguchi, Y., et al. (2007). RAD18 and poly(ADP-ribose) polymerase independently suppress the access of nonhomologous end joining to double-strand breaks and facilitate homologous recombinationmediated repair. *Molecular and cellular biology, 27*(7), 2562-2571.

Sakane, K. K., Monteiro, C. J., Silva, W., Silva, A. R., Santos, P. M., Lima, K. F., and Moraes, K. C. M. (2014). Cellular and molecular studies of the effects of a selective COX-2 inhibitor celecoxib in the cardiac cell line H9c2 and their correlation with death mechanisms. *Brazilian Journal of Medical and Biological Research, 47*(1), 50–59. doi: 10.1590/1414-431X20133028

Sakata, K., Kashiwagi, K., Sharmin, S., Ueda, S., Irie, Y., Murotani, N., and Igarashi, K. (2003). Increase in putrescine, amino oxidase, and acrolein in plasma of renal failure patients. *Biochemical and Biophysical Research Communications, 305*(1), 143-149.

Samol, J., Ranson, M., et al. (2011). Safety and tolerability of the poly (ADP-ribose) polymerase (PARP) inhibitor, olaparib (AZD2281) in combination with topotecan for the treatment of patients with advanced solid tumors: a phase I study. *Investigational New Drugs, 30*(4), 1493-1500.

Sardão, V.A., Oliveira, P.J., Holy, J., Oliveira, C.R., and Wallace, K.B. (2007). Vital imaging of H9c2 myoblasts exposed to tert-butylhydroperoxide—characterization of morphological features of cell death. *BMC Cell Biology, 8*(11). doi: 10.1186/1471-2121-8-11

Satoh, M. S., Poirier, G. G., and Lindahl, T. (1994). Dual function for poly(ADP-ribose) synthesis in response to DNA strand breakage. *Biochemistry, 33*(23), 7099-7106.

Shakir, D. K. & Rasul, K. I. (2009). Chemotherapy induced cardiomyopathy: Pathogenesis, monitoring and management. *Journal of Clinical Medicine Research, 1*(1), 8-12.

Simbulan-R., C.M., Rosenthal, D.S., Luo, R., Samara, R., Espinoza, L.A., Hassa, P.O., Hottiger, M.O., and Smulson, M.E. (2003). PARP-1 binds E2F-1 independently of its DNA binding and catalytic domains, and acts as a novel coactivator of E2F-1-mediated transcription during re-entry of quiescent cells into S phase. *Oncogene, 22*(52), 8460 8471.

Sosna, J., Voigt, S., Mathieu, S., Lange, A., Thon, L., Davarnia, P., et al. (2014). TNF-induced necroptosis and PARP-1-mediated necrosis represent distinct routes to programmed necrotic cell death. *Cellular and Molecular Life Sciences, 71*(2), 331–348. doi:10.1007/s00018-013-1381-6

Sthijns, M. M., Randall, M. J., Bast, A., and Haenen, G. R. (2014). Adaptation to acrolein through upregulating the protection by glutathione in human bronchial epithelial cells: the materialization of the hormesis concept. *Biochemical and Biophysical Research Communications, 446*(4), 1029-1034.

Studzian, K., Kik, K., Lukawska, M., Oszczapowicz, I., Strek, M., and Szmigiero, L. (2015). Subcellular localization of anthracyclines in cultured rat cardiomyoblasts as possible predictors of cardiotoxicity. *Investigational New Drugs, 33*(5), 1032-1039.

Swindall, A. F., Stanley, J. A., and Yang, E. S. (2013). PARP-1: Friend or Foe of DNA Damage and Repair in Tumorigenesis? *Cancers, 5*(3), 943–958. doi: 10.3390/cancers5030943

Szabó, C. (2005). Cardioprotective effects of poly (ADP-ribose) polymerase inhibition. *Pharmacological Research, 52*, 34-43.

Tanel, A., and Averill-Bates, D. A. (2005). The aldehyde acrolein induces apoptosis via activation of the mitochondrial pathway. *Biochimica et Biophysica Acta, 1743*, 255-267. Accessed on 2 December 2015 at PMID: 15843039 [PubMed – indexed for MEDLINE].

Tanel, A., and Averill-Bates, D. A. (2007). Inhibition of acrolein-induced apoptosis by the antioxidant N-acetylcysteine. doi:10.1124/jpet.106.114678

Tomita, M., Aoki, Y., & Tanaka, K. (2004). Effect of haemodialysis on the pharmacokinetics of antineoplastic drugs. *Clinical Pharmacokinetics, 43*(8): 515-527.

Torti, FM., Bristow, MM., Lum, BL., et al. (1986). Cardiotoxicity of epirubicin and doxorubicin: Assessment of endomyocardial biopsy. *Cancer Research, 46*, 3722-3727.

Uchida, K., Kanematsu, M., Sakai, K. Matsuda, T., Hattori, N., Mizuno, Y., Suzuki, D., Miyata, T., Noguchi, N., Niki, E., Osawa, T. (1998). Protein-bound acrolein: potentialmarkers for oxidative stress. *Proceedings of the National Academy of Sciences, 95*, 4882–4887.

US FDA. (1959). Highlights of prescribing information: cyclophosphamide. *US Department of Health and Human Services – FDA*, 1-49. Accessed on 23 February 2016 from www.accessdata.fda.gov/drugsatfda_docs. Last updated: 2013.

US FDA. (2009). Hydroquinone: supporting information for toxicological evaluation by the National Toxicology Program. *US Department of Health and Human Services – FDA*, 1-49. Accessed on 4 December 2015 from http://ntp.niehs.nih.gov/.

Van der Putten, H. H. A. G. M., Joosten, B. J. L. J., Klaren, P. H. M., and Everts, M. E. (2002). Uptake of tri-iodothronine and thyroxine in myoblasts and myotubes of the embryonic heart cell line H9c2(2-1). *Journal of Endocrinology, 175*, 587-596.

Virág, L., Salzman, A. L., and Szabó, C. (1998). Poly(ADP-ribose) synthetase activation mediates mitochondrial injury during oxidant-induced cell death. *The Journal of Immunology, 161*, 3753-3759.

Wacker, D. A., Ruhl, D. D., Balagamwala, E. H., Hope, K. M., Zhang, T., and Kraus, W. L. (2007). The DNA binding and catalytic domains of poly(ADP-ribose) polymerase 1 cooperate in the regulation of chromatin structure and transcription. *Molecular and Cellular Biology*, *27*(21), 7475-7485.

Wang, L., Sun, Y., Asahi, M., and Otsu, K. (2011). Acrolein, an environmental toxin, induces cardiomyocyte apoptosis via elevated intracellular calcium and free radicals. *Cell Biochemistry and Biophysics, 61*, 131-136. doi: 10.1007/s12013-011-9169-5

Watkins, S.J., Borthwick, G.M., and Arthur, H.M. (2011). The H9c2 cell line and primary neonatal cardiomyocyte cells show similar hypertrophic responses in vitro. *In Vitro Cellular and Developmental Biology – Animal, 47*(2), 125-131.

Xu, Y., Huang, S., Liu, Z.G., and Han, J. (2006). Poly(ADP-ribose) polymerase-1 signaling to mitochondria in necrotic cell death requires RIP1/TRAF2-mediated JNK1 activation. *The Journal of Biological Chemistry, 281*(13), 8788-8795.

Yamazaki, K. Miwa, S., Ueda, K., Tanaka, S., Toyokuni, S., Unimonh, O., Nishimura, K., and Komeda, M. (2004). Prevention of myocardial reperfusion injury by poly(ADP-ribose) synthetase inhibitor, 3-aminobenzamide, in cardioplegic solution: in vitro study of isolated rat heart model. *European Journal of Cardio-Thoracic Surgery, 26*(2), 270-275.

Yeh, E.T.H., Tong, A.T., Lenihan, D.J., et al. (2004). Cardiovascular complications of cancer therapy: diagnosis, pathogenesis, and management. *Circulation, 109*, 3122-3131.

Zhang, J., Dawson, V. L., Dawson, T. M., & Snyder, S. H. (1994). Nitric oxide activation of poly (ADP-ribose) synthetase in neurotoxicity. Science, *263*(5147), 687-689.

Zhou, H.Z., Swanson, R.A., Simonis, U., Ma, X., Cecchini, G., and Gray, M.O. (2006). Poly(ADP-ribose) polymerase-1 hyperactivation and impairment of mitochondrial respiratory chain complex I function in reperfused mouse hearts. *American Journal of Physiology: Heart and Circulatory Physiology, 291*, H714–H723.

Zong, W. X., Ditsworth, D., Bauer, D. E., Wang, Z. Q., and Thompson, C. B. (2004). Alkylating DNA damage stimulates a regulated form of necrotic cell death. *Genes and Development, 18*, 1272-1282.

APPENDIX 1.

Protocol for Creation of Complete Supplemented Medium

1.1 Purpose

To prepare complete, supplemented cell culture media.

1.2 Scope

This procedure was used to prepare 10% Fetal Bovine Serum supplemented media for H9c2 (2-1) cell culture. The complete, supplemented cell culture media was developed prior to use and stored at 4°C.

1.3 Materials and Reagents

1.3.1 70% EtOH (Denatured) stored at room temperature
1.3.2 Dulbecco's Modified Essential Medium (DMEM) stored in 4°C refrigerator
1.3.3 Fetal Bovine Serum (FBS) stored in -20°C freezer
1.3.4 Penicillin-Streptomycin stored in -20°C freezer
1.3.5 HEPES buffer, stored in 4°C refrigerator

1.4 Procedure

1.4.1 Obtain a 500 mL bottle of DMEM media from refrigerator and warm to room temperature in a water bath of 37°C.
1.4.2 Obtain 10% FBS media, pre-mixed and stored in 50 mL conical vials at -20°C, and warm to room temperature in a water bath of 37°C.
1.4.3 Obtain and warm 100U/mL of penicillin and 100mg/mL of streptomycin to room temperature in a water bath of 37°C.
1.4.4 Obtain 10mM HEPES buffer from refrigerator and warm to room temperature in a water bath of 37°C.
1.4.5 Sterilize all with 70% EtOH (denatured) and place under sterilized hood
1.4.6 Add 5.6 mL 10mM HEPES buffer to 500 mL DMEM
1.4.7 Add 56 mL 10% FBS to supplemented DMEM
1.4.8 Add 5.6 mL penicillin-streptomycin mixture to supplemented DMEM
1.4.9 Lightly agitate container to mix contents
1.4.10 Sterilize, label appropriately, and store at 4°C for future use

APPENDIX 2.

Protocol for Cell Subdivision of Attached Cells

Adapted from Xiaoyuan Kong, M.D. (Dr. Fant Lab, Orig. January 2010)

1.1 Purpose

To appropriately subdivide attached cells for further propagation or experimentation.

1.2 Scope

This procedure was used to subdivide H9c2 (2-1) cardiomyocytes from the embryonic myocardium of *rattus norvegicus*.

1.3 Materials and Reagents

1.3.A 70% EtOH (Denatured) stored at room temperature
1.3.B Dulbecco's Phosphate-Buffered Saline (DPBS) stored at room temperature
1.3.C Dulbecco's Modified Essential Medium (DMEM) stored in a sealed plastic bag in a 4°C refrigerator
1.3.D 0.1% Trypsin EDTA stored in -20°C freezer

1.4 Procedure

1.4.A General Preparation
1.4.A.A UV sterilize for 40 minutes; sterilize hands and don lab gloves
1.4.A.B Obtain a bottle of complete, supplemented DMEM media from 4°C refrigerator and warm to room temperature in a water bath of 37°C.
1.4.A.C Turn on hood vacuum, light, and blower
1.4.A.D Swab inside of hood with 70% EtOH (Denatured)
1.4.A.E Swab microscope stand with 70% EtOH (Denatured)

1.4.B Specific Procedural Preparation
1.4.B.A Swab medium and DPBS with 70% EtOH (Denatured) and place in hood
1.4.B.B <u>0.1% Trypsin EDTA</u>
1.4.B.B.1 Remove from -20°C

1.4.B.B.2 Place in a water bath of 37°C for a few minutes until warm
1.4.B.B.3 Dry container completely
1.4.B.B.4 Swab with 70% EtOH (Denatured) and place in hood
1.4.B.C Remove cells from incubator and place under microscope to check health and confluence, place inside hood

1.4.C Aspirate Old Medium
1.4.C.A Attach 10mL seriological pipette to pipettor
1.4.C.B Extract old media and place into "Cell Culture Waste" container
1.4.C.C Discard pipette, reseal waste container

1.4.D DPBS Rinse
1.4.D.A Attach 5mLor 10mL seriological pipette to pipettor
1.4.D.B Dispense 5mL DPBS to the sides of each Petri dish, or 1mL DPBS to the sides of each well (for 6 well plates)
1.4.D.C Gently rotate in cardinal directions
1.4.D.D Aspirate DPBS from cells and place in waste container
1.4.D.E Discard pipette

1.4.E Trypsinization and Cell Detachment
1.4.E.A Attach 5mLor 10mL seriological pipette to pipettor
1.4.E.B Add 2mL 0.1% Trypsin EDTA to the sides of each Petri dish, or 0.5mL 0.1% Trypsin EDTA to the sides of each well (for 6 well plate) to start trypsinization
1.4.E.C Discard Pipette
1.4.E.D Gently rotate in cardinal directions to evenly cover surface
1.4.E.E Incubate at 37°C for 5 minutes

1.4.F Stop Trypsinization, isolate cells, re-suspend cells
1.4.F.A Remove cells from incubator
1.4.F.B Add 5mL DMEM to the sides of each Petri dish to stop Trypsinization, or 1mL DMEM to the sides of each well (for 6 well plates) to stop the reaction
1.4.F.C Transfer to sterile 15mL conical centrifuge tube(s), washing wells with medium to ensure all cells are collected
1.4.F.D Label conical tube(s) and discard pipette
1.4.F.E Place tube(s) into Whisperfuge and balance appropriately
1.4.F.F Centrifuge at room temperature for 5 minutes at 125 x g
1.4.F.G During centrifugation, prepare new Petri dishes or plates and add appropriate volumes of DMEM
1.4.F.H Remove tubes from centrifuge and place back into hood
1.4.F.I Attach sterile pipette to pipettor
1.4.F.J Aspirate supernatant, making sure the pellet is not touched

1.4.G Subdivide or Freeze for long-term storage
1.4.G.A If archiving cells
1.4.G.A.1 Reconstitute pellet with 1mL freezing medium, place in sterilized cryo tube (1.0 – 1.3mL per cryo tube), store in freezer at -80°C

1.4.G.B If subdividing

1.4.G.B.1 Add 5mL Media to 15mL conical tube(s) and mix thoroughly to re-suspend pellet

1.4.G.B.2 Distribute suspended cells into Petri dishes or wells

1.4.G.B.3 Note: If cells are to be separated into Petri dishes or multi-well plates with a predetermined concentration (e.g., for experimentation), cells must be counted via Hemocytometer (Refer to Trypan Blue Exclusion Protocol)

1.4.G.C Gently rotate in Cardinal directions to evenly distribute cells

1.4.H Clean-up

1.4.H.A Check cells with microscope, and return to 37°C incubator

1.4.H.B Close and sterilize all media/reagent bottles with 70% EtOH (Denatured), wrap in Parafilm, sterilize with 70% EtOH (Denatured) and return to the appropriate storage location (found in Appendix 2 Section 1.3)

1.4.H.C Sterilize hood surface with 70% EtOH (Denatured)

1.4.H.D Turn off light and blower in hood

1.4.H.E Turn off water bath

1.4.H.F UV sterilize for 40 minutes

1.4.H.G Remove gloves and wash-up

APPENDIX 3.

Protocol for Acrolein and Hydroquinone Exposures

1.1 Purpose

To exposure cells to acrolein and hydroquinone in a safe and effective manner.

1.2 Scope

This procedure was used to expose H9c2 (2-1) cardiomyocytes from the embryonic myocardium of *rattus norvegicus* to acrolein and hydroquinone.

1.3 Materials and Reagents

1.3.A 70% EtOH (Denatured) stored at room temperature
1.3.B Acetone-hexane mixture for sterilization
1.3.C Dulbecco's Phosphate-Buffered Saline (DPBS) stored at room temperature
1.3.D Dulbecco's Modified Essential Medium (DMEM) stored in a sealed plastic bag in a 4°C refrigerator
1.3.E Triton X-100
1.3.F PARP 10X buffer, stored at room temperature
1.3.G 1mM DTT, stored at 4°C
1.3.H 1mM PMSF
1.3.I 400 mM NaCl, stored at 4°C
1.3.J 0.3% hydroquinone solid, stored at room temperature
1.3.K Acrolein, stored under inert conditions
1.3.K.A Molecular Weight of Acrolein = 56.06 g/mol
1.3.L Nitrogen air, stored at room temperature
1.3.M ddH_2O, ultrapure H_2O, stored at 4°C

1.4 Preparation

1.4.A General Preparation
1.4.A.A UV sterilize for 40 minutes; sterilize hands and don lab gloves.
1.4.A.B Obtain a bottle of complete, supplemented DMEM media from 4°C refrigerator and warm to room temperature in a water bath of 37°C.
1.4.A.C Turn on hood vacuum, light, and blower.
1.4.A.D Swab inside of hood with 70% EtOH (Denatured).

1.4.A.E Gather all appropriate materials for experimentation, and appropriately sterilize and place in exact locations for use.

1.4.B Preparation of 1x Lysis Buffer

1.4.B.A Calculate the total volume needed based on acrolein-treated samples, hydroquinone-treated samples, and lysis buffer controls

1.4.B.B Add 0.9% of the total volume calculated in 1.4.B.A of Triton X-100 to a 10mL previously-autoclaved conical vial.
Note: we use 0.9% because there is already 0.1% triton X-100 in the PARP 10x buffer which will be added in step 1.4.B.D

1.4.B.C Warm NaCl (400 mM) to room temperature and then add 10% of the total volume calculated in 1.4.B.A of NaCl to the 10mL vial (e.g., 400µL if making 4mL 1x lysis buffer).

1.4.B.D Add 10% of the total volume calculated in 1.4.B.A of 10X PARP buffer to the 10mL vial (e.g., 400µL if making 4mL 1x lysis buffer).
Note: if 10X PARP buffer needs to be mixed, see Protocol for Poly (ADP-Ribose) Polymerase Assay.

1.4.B.E Set on ice.
Note: Immediately before use, add DTT and PMSF

1.4.C Preparation of Vials for Sample Collection

1.4.C.A Label and organize appropriate number of previously-autoclaved 0.5mL vials for PARP assay

1.4.C.B Label and organize appropriate number of previously-autoclaved 0.5mL vials for protein quantification

1.4.C.C Add 75µL saline into the protein quantification "unknown" vials.

1.4.D Preparation of Control Dilution (0.3% hydroquinone solution)

1.4.D.A Calculate the final volume needed using total number of wells and assuming 200µL of loss per well using the general formula: Final volume of solution = 200 µL for control wells x (# of control wells) x 2 (to account for loss)

1.4.D.B Weigh a previously-autoclaved 2.5 mL vial
Weigh out 0.006g of hydroquinone and dilute with ultrapure dH_2O until volume is equal to the calculated final volume.

1.4.E Preparation of Inert Conditions

1.4.E.A Sterilize needles with acetone-hexane mixture, allow time to air-dry

1.4.E.B Prepare and label a 0.5 mL collection tube

1.4.E.C Obtain 10 cc syringe with needle end attached and flush out ambient air a few times and place tip into a cork

1.4.E.D Prepare 2 nitrogen-filled balloons. Using ambient air pump, fill the balloons a few times, allowing them to deflate in order to stretch latex.

1.4.E.E Fill balloon with nitrogen gas: after inserting nitrogen plastic tube into balloon, twist balloon to prevent leaks and fill with nitrogen.

1.4.E.F Remove balloon from nitrogen plastic tube and twist

1.4.E.G Insert open end of 10cc syringe into balloon and move balloon up tube

1.4.E.H Allow balloon to untwist.

1.4.E.I Crimp top onto new container, insert blue-tipped venting needle and insert needle attached to nitrogen balloon. Check to ensure air is leaving from the blue-tipped needle. Leave for 10 mins to allow nitrogen to displace ambient air.

1.4.E.J Repeat for second balloon and insert this one into acrolein-container (no venting needle needed).

1.5 Procedure

1.5.A Acrolein Extraction

1.5.A.A Attach 10 µL syringe to the 12" dosing needle with parafilm.

1.5.A.B Flush dosing needle with ambient air twice and then flush with nitrogen air (pull up 10 µL nitrogen from new container, expel into open air. Repeat).

1.5.A.C Insert dosing needle into acrolein, pull up 10 µLVERY SLOWLY, and then halfway remove the dosing needle until the tip is in air (still in acrolein bottle). Pull up about 4 µL air VERY SLOWLY from acrolein container.

1.5.A.D Remove needle from acrolein container and dispense into the 0.5 mL stock vial which will be used for experiment.

1.5.A.E Secure, sterilize, and replace acrolein stock storage container and needles to their appropriate storage locations.

1.5.B Preparation of Acrolein Dilutions

1.5.B.A Pipette 499.5µL ddH_2O into previously-autoclaved 1.5mL stock vial

1.5.B.B Extract 0.5µL acrolein from the 0.5mL stock vial and place into the 1.5mL vial containing the ddH_2O. Homogenize.

1.5.B.C Extract 4.73µL of the acrolein-ddH_2O solution from the 1.5mL vial and add to 5mL warmed DMEM.

1.5.B.D Progress through serial dilution for both acrolein and the 0.3% hydroquinone solution to obtain correct concentrations for the current trial. In this experiment, concentrations of 50µM, 75µM, 100µM, and 125µM were needed.

1.5.C Exposure of Cells to Acrolein

1.5.C.A Working with one row or column at a time, remove media from wells and place in regular waste container.

1.5.C.B Wash wells with 400µL DPBS per well, gently rotating in cardinal directions and then extracting and placing in regular waste container.

1.5.C.C Add appropriate concentration of 200µL of hydroquinone stock solution in ddH_2O to each well for the control wells.

1.5.C.D Add appropriate concentration of 200µL acrolein stock solution in ddH_2O to each well for the acrolein-exposed wells.

1.5.C.E Move trays in cardinal directions and then incubate in a humidified atmosphere of 5% CO_2 at 37°C for the appropriate timing for each plate (either 25 minutes, 55 minutes, or 75 minutes, depending on the plate and trial).

1.5.D Finish 1x Lysis Buffer Preparation

1.5.D.A Obtain the 10mL vial containing most of the 1x lysis buffer ingredients that was incubated on ice.

1.4.E.K Add 0.1% 1mM DTT of the total volume calculated in 1.4.B.A to the 10mL vial (e.g., 4µL if making 4mL 1x lysis buffer).

1.4.E.L Add 0.5% 1mM PMSF of the total volume calculated in 1.4.B.A to the 10mL vial (e.g., 20µL if making 4mL 1x lysis buffer).

1.5.D.B Fill the 10mL vial up to the 2mL mark with chilled ddH_2O

1.5.D.C Gently homogenize.

1.5.E Isolate Proteins and Extract Lysate

1.5.E.A Working with one row or column at a time, extract contents from wells and place in hazmat acrolein P450 waste container.

1.5.E.B Wash wells with 200µL DPBS and put in hazmat acrolein P450 waste container.

1.5.E.C Add 75µL of the 1x lysis buffer to each well.

1.5.E.D Repeat for all wells on the plate and then cover the plate.

1.5.E.E Tap plate and incubate on ice for 30 mins

1.5.E.F While the plate is incubating on ice: prepare the lysis buffer control in previously-autoclaved 0.5mL vials by adding 150µL of 1x lysis buffer control to a 0.5mL vial for protein quantification and adding 150µL of 1x lysis buffer control to a 0.5mL vial for PARP assay. Place on ice.

1.5.E.G Working over ice, remove lysate from wells after 30 minutes incubation and place into labeled PARP tubes. Extract 7.5µL from the PARP tube and place in the corresponding protein quantification vial for each sample.

1.5.E.H Store the PARP assay vials, including the 0.5mL tube containing 75µL lysis buffer control, in the -80°C freezer.

1.5.E.I Store the protein quantification vials, including the 0.5mL tube containing 75µL lysis buffer control, in the -20°C freezer. Skip this step and proceed to the Protocol for Bicinchoninic Acid (BCA) Protein Assay if performed on the same day

1.6 Clean-up

1.6.A Close and sterilize all containers with 70% EtOH (Denatured), wrap in Parafilm, sterilize with 70% EtOH (Denatured) and return to their appropriate storage locations.

1.6.B Turn off water bath.

1.6.C Secure acrolein P450 hazardous waste container and place in storage locker.

1.6.D Replace all materials in the hood to their proper locations and then sterilize hood surface with 70% EtOH (Denatured). Turn off light and blower in hood.

1.6.E UV sterilize for 40 minutes.

1.6.F Sterilize any other hood surfaces used with 70% EtOH (Denatured) (e.g., hood surface where acrolein was extracted from stock storage container).

1.6.G Remove gloves and wash-up.

APPENDIX 4.

Protocol for Bicinchoninic Acid (BCA) Protein Assay

Adapted from Xiaoyuan Kong, M.D. (Dr. Fant Lab, Orig. October 2010) for Pierce BCA Protein Quantification Assay

1.1 Purpose

To determine protein concentrations.

1.2 Scope

This procedure was used to determine the amount of protein present after exposure of H9c2 (2-1) cardiomyocytes from the embryonic myocardium of *rattus norvegicus* to acrolein.

1.3 Materials and Reagents

1.3.A 70% EtOH (Denatured) stored at room temperature
1.3.B Lysis buffer control, stored temporarily at -4°C
1.3.C Protein standards, or 0.2% Bovine Serum Albumin (BSA) if protein standards need to be made
1.3.D Unknown samples, stored in freezer at -80°C
1.3.E Pierce BCA reagent A, containing sodium carbonate, sodium bicarbonate, bicinchoninic acid and sodium tartrate in 0.1M sodium hydroxide, stored at room temperature
1.3.F Pierce BCA reagent B, containing 4% cupric sulfate, stored at room temperature

1.4 Procedure

1.4.A General Preparation: can occur on a day prior to running the assay
1.4.A.A Calculate working reagent volumes
1.4.A.A.1 **Reagent A:** Determine the number of standards, the number of unknowns, and the number of controls and blanks and add them together. Then multiply by the number of replicates (i.e., 2) and appropriate volume per sample (i.e., 400μL) to account for potential loss
1.4.A.A.2 **Reagent B:** Divide the volume obtained for reagent A by 50 to obtain a ratio of 50:1, Reagent A:B
1.4.A.B Set up MicroQuant spectrophotometer for absorbance to be read at 562 nm

1.4.A.C Working under UV sterilized and 70% EtOH (Denatured) sterilized conditions with sterilized hands and lab gloves, turn on non-cell culture incubator and allow it to warm to 37°C

1.4.A.D Obtain previously-frozen unknown samples from the -80°C freezer and keep them on ice.

1.4.B Protein Standard Preparation

1.4.B.A **If pre-prepared:** obtain prepared samples from the -20 C freezer and keep on ice. Proceed to step 1.5.

1.4.B.B **If not pre-prepared:**

1.4.B.B.1 Prepare serial dilutions of 0.2% BSA with the buffer for standard BSA concentrations of 2,000 µg/mL, 1,000 µg/mL, 500 µg/mL, 250 µg/mL, 125 µg/mL, 62.5 µg/mL, 31.25 µg/mL, and 15.63 µg/mL and keep on ice.

1.4.B.C Combine reagent A and reagent B in 50mL sterile conical vial in appropriate volumes, as calculated in 1.4.A.A, to create the working reagent. Vortex. Keep on ice and dispense within 5 minutes of preparation.

1.4.C 96-well Plate Procedure

1.4.C.A Pipette 25 µL of each protein standard or unknown sample into the 96-well plate in duplicates, making sure to manually mix each sample beforehand.

1.4.C.B Vortex and then pipette 25 µL of the lysis buffer control into the 96-well plate in duplicates.

1.4.C.C Pipette 200 µL of working reagent to each well, making sure to vortex the reagent before plating for each duplicate.

1.4.C.D Lightly tap plate for 5 seconds to ensure dispersion of contents across entire well.

1.4.C.E Cover plate and incubate in the non-cell culture incubator at 37°C for 30 minutes.

1.4.C.F Remove plate and allow it to cool to room temperature while covered

1.4.C.G Measure absorbance at 562 nm using the BioTek µQuant spectrophotometer.

1.5 Clean-up

1.5.A Close and sterilize BSA container with 70% EtOH (Denatured), wrap in Parafilm, sterilize with 70% EtOH (Denatured) and return to 4°C refrigerator (if to be used within 7 days) or to the -20°C freezer (for future use).

1.5.B Replace other reagents to proper locations; turn off incubator.

1.5.C Discard of the 96-well plate in a hazardous materials waste receptacle.

1.5.D Clean up and sterilize work bench.

APPENDIX 5.

Protocol for Poly(ADP-Ribose) Polymerase Assay

1.1 Purpose

To determine poly (ADP-ribose) polymerase-1 (PARP-1) activity.

1.2 Scope

This procedure was used to measure the amount of PARP activity present in cell lysate protein after exposure of H9c2 (2-1) cardiomyocytes from the embryonic myocardium of *rattus norvegicus* to acrolein.

1.3 Materials and Reagents for Day 1 (Histone Plating)

1.3.A 70% EtOH (Denatured) stored at room temperature
1.3.B Histone stock solution, stored at -20°C
1.3.C Sodium carbonate ($NaCO_3$), powder, stored at room temperature
1.3.D Sodium bicarbonate ($NaHCO_3$), powder, stored at room temperature
1.3.E ddH_2O

1.4 Procedure for Day 1 (Histone Plating)

1.4.A Mix 5mL of 100mM bicoarbonate [190 mM Na^+] buffered histone plating solution
Note: the following is calculated per 96-well plate, adjust measurements accordingly for the number of plates the assay will be run on.

1.4.A.A Weigh out 48mg $NaCO_3$ in a previously-autoclaved 15mL conical vial.
1.4.A.B Add 4.3mg $NaHCO_3$ to a previously-autoclaved 1.5mL vial.
1.4.A.C Add enough ddH_2O to the 1.5mL vial so that a total volume of 1mL is reached. Vortex and then add to the 15mL conical vial.
1.4.A.D Add enough ddH_2O to the 15mL conical vial so that a total volume of 5mL is reached. Vortex.
1.4.A.E Add 500µL histone stock solution to the 15mL conical vial.
1.4.A.F Vortex on high and slowly decrease speed to ensure maximum solubilization.
1.4.A.G Keep on ice.

1.4.B Plate Histones

1.4.B.A Obtain a non-sterile binding assay plate and place on an icepack with a piece of parafilm separating the two in order to prevent scratching of the plate.

1.4.B.B Obtain histone plating solution and vortex it for 5 seconds.

1.4.B.C Add 50µL of Histone Plating Solution to each well, remembering to recap and vortex solution for 3-5 seconds after plating every 5 wells. Add the solution to the center of the well, straight down, in order to effectively coat the entire bottom of each well with histone plating solution. DO NOT FORM BUBBLES.

1.4.B.D Tap plate gently and then rotate in cardinal directions in order to distribute histone solution until each bottom surface of each well is completely covered with histone plating solution.

1.4.B.E Tap plate gently for an additional 10 seconds.

1.4.B.F Seal the open surface of the plate with parafilm so that no air is trapped in order to minimize evaporation. Leave parafilm on bottom to prevent scratching of plate.

1.4.B.G Label plate and place a white plastic tray over top to ensure parafilm doesn't pop up. Record time.

1.4.B.H Refrigerate plate at 4°C overnight.

1.5 Clean-up for Day 1 (Histone Plating)

1.5.A $NaCO_3$ and $NaHCO_3$ containers should have been re-capped and stored in proper cabinet upon finishing weighing procedure.

1.5.B Properly dispose of all other containers.

1.5.C Sterilize precision scale and work bench.

1.6 Materials and Reagents for Day 2 (Blocking Step)

1.6.A 70% EtOH (Denatured) stored at room temperature

1.6.B Dulbecco's Phosphate-Buffered Saline (DPBS) stored at room temperature

1.6.C 0.05% Tween-20

1.6.D 10% Stock Bovine Serum Albumin (BSA)

1.6.E Magnesium Chloride ($MgCl_2 \cdot 6H_2O$), solid, or aqueous $MgCl_2 \cdot 6H_2O$ if pre-mixed and stored in refrigerator at 4°C

1.6.F Triton X-100

1.6.G Tris Base, powder

1.6.H Hydrochloric Acid (HCl)

1.6.I Autoclaved ultrapure H_2O

1.7 Procedure for Day 2 (Blocking Step)

1.7.A General Preparation: can occur on the day prior to running day 2 (blocking step) of the PARP assay or can be done on the same day

1.7.A.A Calculate dilution volumes by analyzing protein quantification data and normalizing against the standard curve.

1.7.A.B Make 10X PARP buffer

Note: the following numbers will produce 10X PARP buffer solution with a total volume of 4mL. Adjust numbers for the amount required.

1.7.A.B.1 Weigh out 242.2 mg tris base in a previously-autoclaved 15mL sterile conical vial. Dissolve in 2.5mL ultrapure dH_2O.

1.7.A.B.2 Add 656µL of 1.78M HCl to 15mL vial.

1.7.A.B.3 Set pipette to 40µL. Use 70% EtOH (Denatured) to sterilize scissors. Add tip to pipette then use the sterilized scissors to cut the end of the pipette tip. Transfer 40µL of triton X-100 to the 15mL vial, by continuously drawing up and ejecting the mixture into the 15mL vial.

1.7.A.B.4 Add 202.8µL BSA to 15mL vial.

1.7.A.B.5 Add 160µL $MgCl_2 \cdot 6H_2O$, in the aqueous form, to the 15mL vial.

1.7.A.B.6 Add ultrapure dH_2O to the 15mL vial until a volume of 4mL is reached.

1.7.A.B.7 Vortex 10X PARP buffer solution until detergent is thoroughly mixed in.

1.7.A.B.8 Sterilize vial and place in -20°C freezer for use tomorrow.

1.7.B Make Phosphate Buffered Saline Supplemented with Tween-20 (i.e., PBS-T) at 0.05%

1.7.B.A Divide a fresh 500mL bottle of DPBS into two sections (each with 250mL).

1.7.B.B Add 125µL of tween-20 into one of the bottles. Re-cap. Lightly agitate and set aside.

1.7.B.C Re-cap and sterilize the other 250mL of untreated DPBS for storage.

1.7.C Make 3% BSA Blocking Buffer

Note: the following is calculated per 96-well plate, adjust measurements accordingly for the number of plates the assay will be run on.

1.7.C.A Obtain pre-made blocking buffer (10%, in DPBS) from 4°C refrigerator. Extract 3mL and add to a previously-autoclaved 15mL conical vial.

1.7.C.B Extract 7mL 1X DPBS and add to the 15mL vial.

1.7.C.C Cap the solution, invert it, and place on ice.

1.7.D Washing Step

Note: Perform the following steps for each plate.

1.7.D.A Remove plate from 4°C refrigerator after overnight incubation.

1.7.D.B Expel contents into sink by inverting the plate above the sink basin. *Rapid.

1.7.D.C Tap plate 5 times on KimWipes to dry the wells. *Rapid.

1.7.D.D Perform wash regime using multichannel pipettes

1.7.D.D.1 Set timer to 5 minutes.

1.7.D.D.2 Wash 1/2: add 200µL PBS-T to each well. Mix plate by lighting tapping with fingers for 10 seconds. Incubate at room temperature for five minutes, tapping plate for 10 seconds on every minute. Change KimWipes with every wash.

1.7.D.D.3 Expel contents into sink by inverting plate above sink basin. *Rapid.

1.7.D.D.4 Repeat step 1.7.D.D.2 and change out pipette tips on multichannel pipette.

1.7.D.D.5 Expel contents into sink by inverting plate above sink basin. *Rapid.

1.7.D.D.6 Wash 3/4: add 200µL DPBS to each well using multichannel pipette. Mix plate by lighting tapping with fingers for 10 seconds. Incubate at room

temperature for five minutes, tapping plate for 10 seconds on every minute. Change KimWipes with every wash.

1.7.D.D.7 Expel contents into sink by inverting plate above sink basin. *Rapid.

1.7.D.D.8 Repeat step 1.7.D.D.6

1.7.D.D.9 After the final DPBS wash, invert plate above sink basin, place face-down on KimWipe for 3 seconds, then tap 5 times to remove contents.

1.7.D.D.10 Add 100µL of the 3% BSA Blocking Buffer to each well using a multichannel pipette.

1.7.D.D.11 Tap plate for 10 seconds to mix, seal with parafilm (wrap completely, leaving the protective plastic sheath or parafilm on the bottom of the plate in order to eliminate scratching.

1.7.D.D.12 Incubate overnight in 4°C refrigerator. Record time.

1.8 Clean-up for Day 2 (Blocking Step)

1.8.A Close and sterilize Triton X-100 and aqueous $MgCl_2 \cdot 6H_2O$ containers with 70% EtOH (Denatured), wrap in Parafilm, sterilize with 70% EtOH (Denatured) and return to proper storage locations and temperatures.

1.8.B Replace other reagents to proper locations.

1.8.C Autoclave 10mL (per plate) of ultrapure dH_2O overnight for day 3 (PARP Activity Detection) experimentation.

1.8.D Clean up and sterilize work bench.

1.9 Materials and Reagents for Day 3 (PARP Activity Detection)

1.9.A 70% EtOH (Denatured) stored at room temperature

1.9.B Dulbecco's Phosphate-Buffered Saline (DPBS) stored at room temperature

1.9.C Autoclaved ultrapure dH_2O

1.9.D 0.05% Tween-20

1.9.E 10X PARP Buffer, created yesterday and stored at -20°C in freezer

1.9.F PARP Enzyme-High Specific Activity (HSA) Standards, stored at -20°C

1.9.G 10X PARP Cocktail solution, stored in freezer at -80°C

1.9.H 10µg/µL of Sheared Herring Sperm DNA, stored in freezer at -80°C

1.9.I biotinylated-NAD, stored at -20°C

1.9.J Unknown samples, stored in freezer at -80°C

1.9.K 10X Strep Diluent

1.9.L 1.25 mg/mL Streptavidin-HRP

1.9.M TMB (3,3',5,5'-tetramethylbenzidine), stored at 4°C

1.9.N 0.2M Stop HCl, stored at room temperature

1.10 Procedure for Day 3 (PARP Activity Detection)

1.10.A Make Phosphate Buffered Saline Supplemented with Tween-20 (i.e., PBS-T) at 0.05%

1.10.A.A Add 125µL of tween-20 into the untreated 250mL DPBS from yesterday. Re-cap. Lightly agitate and set aside.

1.10.B Make 1X PARP Buffer

1.10.B.A Dilute down 10X PARP buffer made yesterday or create new 10X PARP buffer and then dilute down to 1X PARP buffer.

1.10.C Prepare PARP Enzyme-High Specific Activity (HSA) Standards

Note: the following is calculated per 96-well plate, adjust measurements accordingly for the number of plates the assay will be run on.

1.10.C.A Calculate the amount of 1X PARP Buffer required for dilution of samples and standards.

1.10.C.B Label previously-autoclaved sterile 0.5mL vials as 10 units/well (u/w), 5 u/w, 2.5u/w, 1u/w, 0.5 u/w, 0.05u/w, 0.01u/w and BLANK. Place vials on ice.

1.10.C.C Add appropriate volumes of 1X PARP Buffer to corresponding vial, making sure to keep the vials on ice:

PARP Standards	1X PARP Buffer (in µL)
10 units/well	191.67
5 units/well	100
2.5 units/well	100
1.0 units/well	120
0.5 units/well	100
0.05 units/well	135
0.01 units/well	120
BLANK	0

1.10.C.D Dilute PARP HSA Standards

Note: A unit is the amount of enzyme required to catalyze 1µmol of substrate to its final product in a time of 60 seconds.

1.10.C.D.1 Add 8.33µL of the pre-made PARP HSA Standard to the 10 units/well vial. Agitate.

1.10.C.D.2 Take 100µL from the 10 units/well vial and add to the 5 units/well vial. Agitate.

1.10.C.D.3 Take 100µL from the 5 units/well vial and add to the 2.5 units/well vial. Agitate.

1.10.C.D.4 Take 80µL from the 2.5 units/well vial and add to the 1.0 units/well vial. Agitate.

1.10.C.D.5 Take 100µL from the 1.0 units/well vial and add to the 0.5 units/well vial. Agitate.

1.10.C.D.6 Take 15µL from the 0.5 units/well vial and add to the 0.05 units/well vial. Agitate.

1.10.C.D.7 Take 30µL from the 0.05 units/well vial and add to the 0.01 units/well vial. Agitate.

1.10.C.D.8 Remember to keep all vials on ice if not being used. After “step-up” dilution, temporarily store the PARP HSA Standards on ice.

1.10.D Perform Wash Regime Using Multichannel Pipettes (preparing the PARP Cocktail Solution in step 1.10.E as the washes are completed).
Note: Must be repeated individually for each plate.

1.10.D.A Remove Histone-coated plate from 4°C refrigerator.

1.10.D.B Follow steps 1.7.D.D. 1 – 12 for proper wash regime, completing a total of two consecutive rounds for PBS-T and then two consecutive rounds for DPBS (i.e., 4 washes total).

1.10.E Prepare Working PARP Cocktail Solution (Immediately Prior to Use)
Note: the following is calculated per 96-well plate, adjust measurements accordingly for the number of plates the assay will be run on.

1.10.E.A Thaw 10X PARP Cocktail solution on ice.
Note: this solution contains both NAD^+ and biotinylated-NAD at predetermined concentrations; the sum of both in the 1X working reagent is 3mM.

1.10.E.B Dilute the 10X PARP Cocktail with autoclaved ultrapure dH_2O in a 1:10 ratio in a 15mL vial.

1.10.E.C Dilute the 10µg/µL Sheared Herring Sperm DNA stock in a 1:10 ratio with 1X PARP Buffer, mixing gently by pipetting

1.10.E.D Aliquot 20µL of the 1:10 dilution of Sheared Herring Sperm DNA:1X PARP 1X Buffer into the 15mL vial containing the 1X PARP Cocktail solution. Discard any remaining diluted DNA.

1.10.E.E Add the biotinylated-NAD as late as possible to decrease degradation (36µL per pate).

1.10.E.F Vortex cocktail to mix.

1.10.F Plate Standards and Biological Samples
Note: Must be repeated for each plate.

1.10.F.A Remove 96-well plate from ice pack.

1.10.F.B Gently mix PARP HSA Standards and then add 25µL to respective wells in triplicate.

1.10.F.C Gently mix biological samples and then add 25µL to respective wells in triplicate.

1.10.F.D Add 25µL of 1X PARP Cocktail solution to each well using a multichannel pipette. Tap plate for 10 seconds to ensure dispersion of solution across surface.

1.10.F.E Incubate plate (covered) for 60 minutes at room temperature.

1.10.G Prepare Streptavidin-HRP Substrate
Note: Start this preparation with 20 minutes left on incubation from last step.

1.10.G.A Prepare 1X Strep-diluent:

1.10.G.B Combine 9944.3µL PBS-T with 50.7µL BSA for a total volume of 10,000µL (10mL).

1.10.G.C Dilute 99.9µL 10X Strep-HRP Diluent with autoclaved ultrapure dH_2O until a volume of 999µL is achieved.

1.10.G.D Prepare stock streptavidin-HRP solution by adding 1µL of 1.25mg/mL conjugated streptavidin-HRP to 999µL 1X Strep-HRP Diluent. Gently mix. Extract 100µL of this solution and add to 5,900µL of 1X Strep diluent to bring the ratio up to 1:60,000.

1.10.G.E Keep on ice until later use.

1.10.H Perform Wash Regime Using Multichannel Pipettes
Note: Must be repeated individually for each plate.
1.10.H.A Remove Histone-coated plate from 4°C refrigerator.
1.10.H.B Follow steps 1.7.D.D. 1 – 12 for proper wash regime, completing a total of three consecutive rounds for PBS-T and then three consecutive rounds for DPBS (i.e., 6 washes total).
1.10.H.C Remember to change multichannel pipette tips with each wash.

1.10.I Add 1:60,000 Streptavidin-HRP
Note: Must be repeated individually for each plate.
1.10.I.A Add 50µL of 1:60,000 Streptavidin-HRP to each well using a multichannel pipette.
1.10.I.B Mix for 10 seconds by gently tapping plate.
1.10.I.C Incubate plate (covered) at room temperature for 60 minutes.

1.10.J Perform Wash Regime Using Multichannel Pipettes
Note: Must be repeated individually for each plate.
Note: During the last wash, work through steps 1.10.K.A and 1.10.K.B
1.10.J.A Follow steps 1.7.D.D. 1 – 12 for proper wash regime, completing a total of three consecutive rounds for PBS-T and then three consecutive rounds for DPBS (i.e., 6 washes total).
1.10.J.B Remember to change multichannel pipette tips with each wash.

1.10.K Add TMB (3,3',5,5'-tetramethylbenzidine) to Wells
Note: Must be repeated individually for each plate.
Note: TMB is light sensitive!
1.10.K.A Prepare room conditions by turning off lights and protecting TMB from light by wrapping aluminum foil around container. Also wrap 5mL vial in aluminum foil.
1.10.K.B Extract 4,848µL TMB and place into a previously-autoclaved sterile 5mL vial in the dark. Close and sterilize the stock TMB solution and return it to 4°C refrigerator.
1.10.K.C Add 50µL TMB to each well in the dark, remembering to set the timer upon addition of TMB to the first well.
1.10.K.D Incubate plate (covered) at room temperature for 15-20 minutes, depending on color intensity. Color should change from clear to blue.
1.10.K.E Mix 0.2M HCl stock solution during incubation period if insufficient amount (will need approximately 6,500µL per 96-well plate).

1.10.L Add Stop HCl to Wells
Note: Must be repeated individually for each plate.
Note: Must be added in the exact same sequencing as the TMB was added for each well.
1.10.L.A Add 65µL of 0.2M HCl (Stop HCl) to each well.
1.10.L.B Mix contents by gently tapping plate.

1.10.L.C Incubate plate (covered) at room temperature for 10 minutes. Color should change from blue to yellow.

1.10.L.D During incubation time, set up MicroQuant spectrophotometer for absorbance to be read at 562 nm.

1.10.M Measure absorbance at 562 nm using the BioTek μQuant spectrophotometer.

1.11 Clean-up for Day 3 (PARP Activity Detection)

1.11.A Close and sterilize any remaining containers.

1.11.B Replace other reagents to proper locations.

1.11.C Turn off spectrophotometer, remove plate(s) and place into hazardous materials waste receptacle.

1.11.D Clean up and sterilize work bench.